

Manifold functional multiple regression model with LRD error term

Diana P. Ovalle–Muñoz and M. Dolores Ruiz–Medina

Abstract

This paper considers the problem of manifold functional multiple regression with functional response, time-varying scalar regressors, and functional error term displaying Long Range Dependence (LRD) in time. Specifically, the error term is given by a manifold multifractionally integrated functional time series (see, e.g., Ovalle–Muñoz & Ruiz–Medina [53]). The manifold is defined by a connected and compact two-point homogeneous space. The functional regression parameters have support in the manifold. The Generalized Least-Squares (GLS) estimator of the vector functional regression parameter is computed, and its asymptotic properties are analyzed under a totally specified and misspecified model scenario. A multiscale residual correlation analysis in the simulation study undertaken illustrates the empirical distributional properties of the errors at different spherical resolution levels.

Key words: Connected and compact two-point homogeneous spaces, functional regression, LRD manifold functional time series error, manifold correlated curve data, manifold multiple functional regression.

1 Introduction

There exists an extensive literature on functional linear regression given its wide interesting applications in several scientific fields. Among many other contributions, we refer to environmental applications such as air pollution studies (see, e.g., Acal et.al. [2]; Álvarez–Liébana & Ruiz–Medina [6]; Olaya–Ochoa, Ovalle–Muñoz & Urbano–Leon [52]; and references therein), biomechanics applications involving modeling of human movements (see, e.g., in Acal & Aguilera [1]; Helwig et. al. [36]), and epidemiological and brain applications (see, e.g., Aristizabal, Giraldo & Mateu [10]; Yao, Müller & Wang [63]). The main directions of contributions in the above cited references focused on predictive analysis of the

response based on functional regressors in both cases, when response is scalar or functional, as well as in the case where the regression parameters are functions in the parametric framework. In particular, dimension reduction techniques based on functional principal component analysis, constitute a major topic in this literature. Most of the regularization techniques proposed are based on projection into suitable finite-dimensional subspaces, whose dimension depends on the functional sample size. Also suitable weighting operators are considered for embedding the unbounded inverse autocovariance operator of the regressors into the space of bounded linear operators (see, e.g., Bosq [13]; Cardot, Mas & Sarda [16]; Crambes & Ma [21], Mas [50], among others). The main subject of these papers is to remove the ill-posed nature of the associated inverse estimation problem due to unbounded inversion of the autocovariance operator of the functional covariates. Indeed, during the last twenty years several contributors have worked on several numerical proposals for approximation of the slope function, and its asymptotic analysis. The corresponding residual correlation analysis has also been addressed under different scenarios, mainly including the cases of independent or weak-dependent data (see, e.g., Chiou & Müller [18], Shen & Xu [62], among others).

The case of independent functional observations was extensively developed during the first decade of 2000. In particular, regression analysis and inference from a sample of independent and identically distributed functional random variables have been considered in the papers by Crambes, Kneip & Sarda [20]; Cuevas, Febrero & Fraiman [23]; Febrero-Bande, Galeano & Gonzalez-Manteiga [26] (see also Cuevas [22] for an overview). The kernel formulation of the regression parameters is usually adopted in the literature of parametric linear regression with functional response and regressors (see, for example, Chiou, Müller & Wang [19]; Ruiz-Medina (2011) [56]; Ruiz-Medina (2012a) [57]; Ruiz-Medina (2012b) [58], and references therein). An extensive overview, with further references on functional regression approaches, including the case of functional response and regressors, can be as well found in Morris [51]. See also the monograph by Hsing & Eubank [42], where several functional analytical tools are introduced, for estimating random elements in function spaces.

An extended formulation of the previous results to the case of weak-dependent functional observations is provided in the context of functional time series, and in general, of weak-dependent processes. That is the case of approaches based on the concept of L^r - m -approximability to modeling the temporal dependence in the regression functional errors (see, for example, Horváth & Kokoszka [40]). A central topic in this book is the analysis of functional data, displaying dependent structures in time and space. Also, in the framework of weakly dependent functional time series models, supporting inference on stochastic processes, in particular, in a state space framework, several functional regression approaches

have been adopted for functional prediction (see, e.g., Álvarez-Liévana et.al. [4]; Guillas [35]; Hörmann & Kokoszka [38]; Horváth & Kokoszka [40]; Kara-Terki & Mourid [43]; Kokoszka & Reimherr [44]). Confidence bands, kernel and parametric functional time series estimation lead to the analysis of outstanding problems like adaptive bandwidth selection, dimension reduction, change-point analysis, and functional principal component estimation, among others (see, e.g., Berkes, Horváth, & Rice [12]; Dette, Kokot & Aue [24]; Hörmann & Kidzinski [37]; Hörmann & Kokoszka [39]; Horváth, Rice & Whipple [41]; Zhang et.al. [64]).

A fixed effect approach in Hilbert spaces is adopted in Ruiz-Medina [59], for FANOVA analysis under dependent errors. For simple regression, with explanatory variable taking values in some abstract space of functions, the rate of convergence of the mean squared error of the functional version of the Nadaraya-Watson kernel estimator is derived in Benhenni, Hedli-Griche & Rachdi [11], when the errors are represented by a stationary short or long memory process. An alternative approach, based on Autoregressive Hilbertian processes of order 1 (ARH(1)) error term, is presented in Ruiz-Medina, Miranda & Espejo [61] for multiple regression, and in Álvarez-Liévana & Ruiz-Medina [5] for fixed effect models including the case of circular domains.

Classical texts like the book by Ramsay & Silverman [55] have introduced the basic analytical and statistical tools for inference on stochastic processes based on Functional Data Analysis (FDA). The book by Ferraty & Vieu [29] also constitutes a benchmark in the literature on nonparametric functional statistics. In this framework, one can mention, among others, the contributions by Aneiros-Pérez [8], Aneiros-Pérez & Vieu [9], and Ferraty et al. [27], applying, in particular, the Projection Pursuit Regression principle in the approximation of the regression function, for the case of a functional predictor and a scalar response (see also Ferraty & Vieu (2006) [29]; Ferraty & Vieu (2018) [30]). In the nonparametric setting, Ferraty, Keilegom & Vieu [28] derive a kernel type estimator of the regression operator, and its asymptotic normality is proved, for the case of functional response and predictor. Goia & Vieu [33] adopt a semiparametric approach, in a two-terms Partitioned Functional Single Index Model. Several papers on topics related to statistical analysis of high-dimensional data, including functional regression, from the parametric, semiparametric and nonparametric FDA frameworks, can be found in the Special Issue by Goia & Vieu [34].

Recently, an attempt to extend spectral analysis of functional time series to the context of LRD functional sequences has been presented in Ruiz-Medina [60], covering, in particular, some examples of the LRD functional time series family analyzed by Li, Robinson & Shang [46] in the temporal domain. In particular, Li, Robinson & Shang [46] applies Functional Principal Component Analysis (FPCA) based on the long-run covariance function, for the consistent estimation of the dimension and the orthonormal functions spanning the dominant subspace, where

the projected curve process displays the largest dependence range. Fractionally integrated functional autoregressive moving averages processes constitute an interesting example (see Li, Robinson & Shang [46]). The multifractional version of this process family can be analyzed under the modeling framework introduced in Ruiz–Medina [60]. Indeed, in that paper, one can see the important advantages that the application of harmonic analysis entails in this more general context. Particularly, under stationary in time, the temporal dependence range can be approximated from the behavior in a neighborhood of zero frequency of the spectral density operator family at different spatial resolution levels. Moreover, a more flexible modeling framework can be introduced in this setting, allowing the representation of long, intermediate or short range dependence, according to the interval where the pure point or continuous spectrum of the long–memory operator lies (see, e.g., Ovalle–Muñoz & Ruiz–Medina [53]).

In the case of \mathbb{M}_d being a connected and compact two–point homogeneous space with topological dimension d , the invariance of a kernel with respect to the group of isometries of \mathbb{M}_d allows its spectral diagonalization in terms of a fixed orthogonal basis, the eigenfunctions of the Laplace Beltrami operator on the Hilbert space $H = L^2(\mathbb{M}_d, d\nu)$. Here, $d\nu$ denotes the measure induced by the probabilistic invariant measure on the connected component of the group of isometries of \mathbb{M}_d . In the functional time series framework, one can find recent contributions on modeling, estimation and asymptotic analysis of weak–dependent Hilbert–valued processes in the sphere, which constitutes a well–known example of connected and compact two–point homogeneous space (see, e.g., Caponera & Marinucci, [15]; Caponera [14]). Formulation of alternative limit results for sojourn measures of LRD spherical–cross time random fields can be found in Marinucci, Rossi & Vidotto [49]. The reader can see the starting results for manifold analysis based on connected and compact two–point homogeneous spaces in the preliminary contributions on this subject obtained in Ma & Malyarenko [47], for second–order mean–square continuous elliptically contoured random fields on \mathbb{M}_d . Several motivating applications of this modeling framework are given, for example, in Alegría et al. [3], on bayesian multivariate spherical random field modeling from a bivariate spatial data set from two 2019 NCEP/NCAR Flux reanalyses, as well as, in Marinucci & Peccati [48], and Leonenko, Nanayakkara & Olenko [45], in relation to Cosmic Microwave Background (CMB) evolution modeling and data analysis.

The present paper applies the results in Ruiz–Medina [60] and Ovalle–Muñoz & Ruiz–Medina [53] to introduce a new infinite–dimensional linear model family in the context of multiple functional regression models evaluated in a Hilbert space, with finite–dimensional design matrix, and functional response and regression parameters. This paper focuses in the special case of functional error term being an LRD functional time series in the family introduced in Ruiz–Medina

[60]. Thus, compact Riemannian manifold–based residual correlation analysis is addressed here from functional regression parameter estimation when the error term displays LRD. This analysis is achieved from the previous theoretical and numerical results obtained in Ovalle–Muñoz & Ruiz–Medina [53] for LRD functional time series in connected and compact two–point homogeneous spaces. Thus, this paper derives an extended formulation of the linear functional models introduced in Ruiz–Medina [59]; and Álvarez–Liébana & Ruiz–Medina [5], beyond the weak–dependent and Euclidean settings.

The outline of the paper is as follows. Section 2 presents some preliminary elements on the spectral analysis of LRD manifold functional time series. Section 3 introduces our multiple functional regression setting in a parametric framework. The generalized least–squares estimator of the manifold functional regression parameter vector is then computed. In Section 5, a simulation study is undertaken to illustrate the finite–sample and asymptotic properties of the theoretical and empirical functional response predictor. In particular, the effect of the spectral properties of the LRD operator, characterizing the temporal dependence range of the functional error term, on the precision and variability of these response predictors is analyzed. Some final comments and open research lines are discussed in Section 6.

2 Preliminaries

In the regression residual correlation analysis achieved in this paper in the spectral domain, under LRD manifold functional time series error term, invariance of the involved kernels with respect to the group of isometries of \mathbb{M}_d plays a crucial role. Indeed, these kernels are diagonalized by the eigenfunctions $\{S_{n,j}^d, j = 1, \dots, \delta(n, d), n \in \mathbb{N}_0\}$ associated with the eigenvalues $\{\lambda_n = -n\varepsilon(n\varepsilon + \alpha + \beta + 1), n \in \mathbb{N}_0\}$ of the Laplace Beltrami operator Δ_d on $L^2(\mathbb{M}_d, d\nu, \mathbb{R})$ (see, e.g., Cartan [17] and Ma & Malyarenko [47], for more details on Lie Algebra based approach).

We first formulate the addition formula applied in the context of connected and compact two–point homogeneous spaces.

Lemma 1 (See [32, Theorem 3.2.] and [7, p 455]) *For every $n \in \mathbb{N}_0$, the following addition formula holds:*

$$\sum_{j=1}^{\delta(n,d)} S_{n,j}^d(\mathbf{x})S_{n,j}^d(\mathbf{y}) = \frac{\delta(n, d)}{\omega_d} R_n^{\alpha, \beta}(\cos(d_{\mathbb{M}_d}(\mathbf{x}, \mathbf{y}))), \quad \mathbf{x}, \mathbf{y} \in \mathbb{M}_d. \quad (1)$$

Here, $\omega_d = \int_{\mathbb{M}_d} d\nu(\mathbf{x})$, and $\delta(n, d)$ denotes the dimension of the eigenspace \mathcal{H}_n associated with the eigenvalue $\lambda_n = -n\varepsilon(n\varepsilon + \alpha + \beta + 1)$ of the Laplace

Beltrami operator, which is given, for every $n \in \mathbb{N}_0$, by

$$\delta(n, d) = \frac{(2n + \alpha + \beta + 1)\Gamma(\beta + 1)\Gamma(n + \alpha + \beta + 1)\Gamma(n + \alpha + 1)}{\Gamma(\alpha + 1)\Gamma(\alpha + \beta + 2)\Gamma(n + 1)\Gamma(n + \beta + 1)}. \quad (2)$$

Furthermore, $R_n^{\alpha, \beta}(\cos(d_{\mathbb{M}_d}(\mathbf{x}, \mathbf{y}))) = \frac{P_n^{\alpha, \beta}(\cos(d_{\mathbb{M}_d}(\mathbf{x}, \mathbf{y})))}{P_n^{\alpha, \beta}(1)}$, with $P_n^{\alpha, \beta}$ denoting the Jacobi polynomial of degree $n \in \mathbb{N}_0$, with parameters α and β , involved in the definition of $\delta(n, d)$ (see equation (2)).

Let $X = \{X(\mathbf{x}, t), \mathbf{x} \in \mathbb{M}_d, t \in \mathbb{T}\}$ be a zero-mean, stationary in time, and isotropic in space mean-square continuous Gaussian, or elliptically contoured, spatiotemporal random field on the basic probability space (Ω, \mathcal{A}, P) , with covariance function $C(d_{\mathbb{M}_d}(\mathbf{x}, \mathbf{y}), t - s) = E[X(\mathbf{x}, t)X(\mathbf{y}, s)]$, for $\mathbf{x}, \mathbf{y} \in \mathbb{M}_d$, and $t, s \in \mathbb{T}$. Here, \mathbb{T} denotes the temporal domain, which can be \mathbb{Z} or \mathbb{R} . Under the conditions of Theorem 4 in Ma & Malyarenko [47], the covariance function $C(d_{\mathbb{M}_d}(\mathbf{x}, \mathbf{y}), t - s)$ admits the following diagonal series expansion:

$$\begin{aligned} C(d_{\mathbb{M}_d}(\mathbf{x}, \mathbf{y}), t - s) &= \sum_{n \in \mathbb{N}_0} B_n(t - s) \sum_{j=1}^{\delta(n, d)} S_{n, j}^d(\mathbf{x}) S_{n, j}^d(\mathbf{y}) \\ &= \sum_{n \in \mathbb{N}_0} \frac{\delta(n, d)}{\omega_d} B_n(t - s) R_n^{(\alpha, \beta)}(\cos(d_{\mathbb{M}_d}(\mathbf{x}, \mathbf{y}))), \quad \mathbf{x}, \mathbf{y} \in \mathbb{M}_d, t, s \in \mathbb{T}. \end{aligned} \quad (3)$$

Let now $X = \{X(\mathbf{x}, t), \mathbf{x} \in \mathbb{M}_d, t \in [0, T]\}$ be the restriction to the interval $[0, T]$ of a zero-mean, stationary in time, and isotropic in space, mean-square continuous Gaussian, or elliptically contoured, spatiotemporal random field on the basic probability space (Ω, \mathcal{A}, P) , with covariance function $C(d_{\mathbb{M}_d}(\mathbf{x}, \mathbf{y}), t - s)$ admitting the diagonal expansion (3). The following lemma provides the orthogonal expansion of $X = \{X(\mathbf{x}, t), \mathbf{x} \in \mathbb{M}_d, t \in [0, T]\}$ in terms of the eigenfunctions of the Laplace Beltrami operator (see Theorem 1 in the Supplementary Material in Ovalle-Muñoz & Ruiz-Medina [53]).

Lemma 2 *Let $X = \{X(\mathbf{x}, t), \mathbf{x} \in \mathbb{M}_d, t \in [0, T]\}$ be the restriction to the interval $[0, T]$ of a zero-mean, stationary in time, and isotropic in space, mean-square continuous Gaussian, or elliptically contoured, spatiotemporal random field on the basic probability space (Ω, \mathcal{A}, P) , with covariance function (3) satisfying the conditions in Theorem 4 in Ma & Malyarenko [47], with*

$$\sum_{n \in \mathbb{N}_0} B_n(0)\delta(n, d) < \infty. \quad (4)$$

Then, the following orthogonal expansion holds for random field X

$$X(\mathbf{x}, t) \stackrel{\mathcal{L}^2_{\tilde{H}}(\Omega, \mathcal{A}, P)}{=} \sum_{n \in \mathbb{N}_0} \sum_{j=1}^{\delta(n,d)} V_{n,j}(t) S_{n,j}^d(\mathbf{x}), \quad \mathbf{x} \in \mathbb{M}_d, t \in [0, T], \quad (5)$$

where $\mathcal{L}^2_{\tilde{H}}(\Omega, \mathcal{A}, P) = L^2(\Omega \times \mathbb{M}_d \times [0, T], P(d\omega) \otimes d\nu \otimes dt)$, with $\tilde{H} = L^2(\mathbb{M}_d \times [0, T], d\nu \otimes dt)$. Here, $\{V_{n,j}(t), t \in [0, T], j = 1, \dots, \delta(n, d), n \in \mathbb{N}_0\}$ is a sequence of centered random processes on $[0, T]$ given by

$$V_{n,j}(t) = \int_{\mathbb{M}_d} X(\mathbf{y}, t) S_{n,j}^d(\mathbf{y}) d\nu(\mathbf{y}), \quad j = 1, \dots, \delta(n, d), n \in \mathbb{N}_0, \quad (6)$$

in the mean-square sense.

Assume that $\mathbb{T} = \mathbb{Z}$, and that the map

$$\tilde{X}_t : (\Omega, \mathcal{A}) \longrightarrow (L^2(\mathbb{M}_d, d\nu, \mathbb{R}), \mathcal{B}(L^2(\mathbb{M}_d, d\nu, \mathbb{R})))$$

is measurable, with $\tilde{X}_t(\mathbf{x}) := X(\mathbf{x}, t)$ for every $t \in \mathbb{T}$ and $\mathbf{x} \in \mathbb{M}_d$. Here, $\mathcal{B}(L^2(\mathbb{M}_d, d\nu, \mathbb{R}))$ denotes the Borel σ -algebra on $L^2(\mathbb{M}_d, d\nu, \mathbb{R})$ (i.e., the smallest σ -algebra containing the collection of all open subsets of $L^2(\mathbb{M}_d, d\nu, \mathbb{R})$). By previous assumptions on X , $\{\tilde{X}_t, t \in \mathbb{Z}\}$ then defines a manifold stationary functional time series. In particular, $E[\tilde{X}_t] = 0$, and $\sigma_{\tilde{X}}^2 = E[\|\tilde{X}_t\|_{L^2(\mathbb{M}_d, d\nu, \mathbb{R})}^2] = E[\|\tilde{X}_0\|_{L^2(\mathbb{M}_d, d\nu, \mathbb{R})}^2] = \|R_0\|_{L^1(H)}$, for every $t \in \mathbb{Z}$. By $L^1(L^2(\mathbb{M}_d, d\nu, \mathbb{R}))$ we denote the space of trace or nuclear operators on $L^2(\mathbb{M}_d, d\nu, \mathbb{R})$. The second-order structure of $\{\tilde{X}_t, t \in \mathbb{Z}\}$ is characterized by the family of covariance operators $\{\mathcal{R}_t, t \in \mathbb{Z}\}$ given by, for all $h, g \in L^2(\mathbb{M}_d, d\nu, \mathbb{R})$,

$$\mathcal{R}_t(g)(h) = E[\tilde{X}_{s+t}(h)\tilde{X}_s(g)] = E\left[\left\langle \tilde{X}_{s+t}, h \right\rangle_{L^2(\mathbb{M}_d, d\nu, \mathbb{R})} \left\langle \tilde{X}_s, g \right\rangle_{L^2(\mathbb{M}_d, d\nu, \mathbb{R})}\right] \quad (7)$$

with respective kernels

$$r_t(\mathbf{x}, \mathbf{y}) = E[\tilde{X}_{s+t} \otimes \tilde{X}_s](\mathbf{x}, \mathbf{y}), \quad \forall \mathbf{x}, \mathbf{y} \in \mathbb{M}_d, t, s \in \mathbb{Z}.$$

We now introduce some preliminary elements about spectral analysis of functional time series, based on the spectral density operator family, and the periodogram operator, computed from the functional discrete Fourier transform (fDFT) (see, e.g., Panaretos & Tavakoli [54], for the weak-dependent case; Ruiz-Medina [60], Ovalle-Muñoz & Ruiz-Medina [53], for the strong-dependent case).

The functional Fourier transforms of the elements of the family of covariance operators introduced in (7) are here defined in the Hilbert–Schmidt operator norm (see, e.g., Ovalle–Muñoz & Ruiz–Medina [53]). That is, the family of spectral density operators $\{\mathcal{F}_\omega, \omega \in [-\pi, \pi]\}$ characterizing the second–order structure of the functional time series $\{\tilde{X}_t, t \in \mathbb{Z}\}$ in the spectral domain is given by, for each $\omega \in [-\pi, \pi] \setminus \{0\}$:

$$\mathcal{F}_\omega \underset{\mathcal{S}(L^2(\mathbb{M}_d, d\nu, \mathbb{C}))}{=} \frac{1}{2\pi} \sum_{t \in \mathbb{Z}} \exp(-i\omega t) \mathcal{R}_t, \quad (8)$$

where $\underset{\mathcal{S}(L^2(\mathbb{M}_d, d\nu, \mathbb{R}))}{=}$ denotes the identity in the norm of the Hilbert–Schmidt operators. In particular, this identity does not require the summability of the series of trace norms of the elements of the covariance operator family. Equivalently, short–memory is not assumed in our functional time series modeling framework (see, e.g., Panaretos & Tavakoli [54], Ruiz–Medina [60] and Ovalle–Muñoz & Ruiz–Medina [53]).

The fDFT $\tilde{X}_\omega^{(T)}(\cdot)$ of the curve data is defined as

$$\tilde{X}_\omega^{(T)}(\cdot) \underset{L^2(\mathbb{M}_d, d\nu, \mathbb{C})}{=} \frac{1}{\sqrt{2\pi T}} \sum_{t=1}^T \tilde{X}_t(\cdot) \exp(-i\omega t), \quad \omega \in [-\pi, \pi], \quad (9)$$

where $\underset{L^2(\mathbb{M}_d, d\nu, \mathbb{C})}{=}$ denotes the equality in $L^2(\mathbb{M}_d, d\nu, \mathbb{C})$ norm, with $L^2(\mathbb{M}_d, d\nu, \mathbb{C})$ being the complex version of the Hilbert space $L^2(\mathbb{M}_d, d\nu, \mathbb{R})$. Note that $\tilde{X}_\omega^{(T)}(\cdot)$ is a random element in the space $L^2(\mathbb{M}_d, d\nu, \mathbb{C})$, since

$$E \left[\|\tilde{X}_\omega^{(T)}\|_{L^2(\mathbb{M}_d, d\nu, \mathbb{C})} \right] \leq \frac{1}{\sqrt{2\pi T}} \sum_{t=1}^T E \|\tilde{X}_t(\cdot)\|_{\tilde{H}} < \infty.$$

For $\omega \in [-\pi, \pi]$, the periodogram operator $p_\omega^{(T)} = \tilde{X}_\omega^{(T)} \otimes \overline{\tilde{X}_\omega^{(T)}}$ is defined from the fDFT. Its mean is given by convolution of the Féjer kernel $F_T(\omega) = \frac{1}{T} \sum_{t=1}^T \sum_{s=1}^T \exp(-i(t-s)\omega)$ with the spectral density operator. That is,

$$\begin{aligned} E[p_\omega^{(T)}] &= E[\tilde{X}_\omega^{(T)} \otimes \tilde{X}_{-\omega}^{(T)}] = \frac{1}{2\pi} \sum_{u=-(T-1)}^{T-1} \exp(-i\omega u) \frac{(T-|u|)}{T} \mathcal{R}_u \\ &= \int_{-\pi}^{\pi} F_T(\omega - \xi) \mathcal{F}_\xi d\xi, \quad T \geq 2. \end{aligned}$$

3 Multiple Functional regression model

This section introduces our manifold multiple functional regression model in a parametric framework, under an LRD functional time series modelling of the error

term. Specifically, let us consider the following functional observation model in time: For $t = 1, \dots, N$, and $j = 1, \dots, p$,

$$Y_t(\mathbf{x}) = \sum_{j=1}^p X_{t,j} \beta_j(\mathbf{x}) + \varepsilon_t(\mathbf{x}), \quad \mathbf{x} \in \mathbb{M}_d, \quad (10)$$

where $\beta_j \in L^2(\mathbb{M}_d, d\nu, \mathbb{R})$, and $X_{t,j} \in \mathbb{R}$, for $j = 1, \dots, p$, and $t \in \mathbb{Z}$. Here, $\{\varepsilon_t, t \in \mathbb{Z}\}$ defines a stationary LRD functional time series with values in the space $L^2(\mathbb{M}_d, d\nu, \mathbb{R})$ as introduced in the previous section. Note that $\mathbf{X} = (X_{t,j})_{(t,j) \in \{1, \dots, N\} \times \{1, \dots, p\}}$ defines the $N \times p$ design matrix (see also Ruiz–Medina [59]). Equation (10) can be equivalently expressed in vectorial form as follows:

$$\mathbf{Y}(\mathbf{x}) = \mathbf{X}\boldsymbol{\beta}(\mathbf{x}) + \boldsymbol{\varepsilon}(\mathbf{x}) \quad \mathbf{x} \in \mathbb{M}_d, \quad (11)$$

where $\mathbf{Y}(\mathbf{x}) = [Y_1(\mathbf{x}), Y_2(\mathbf{x}), \dots, Y_N(\mathbf{x})]^T$, $\boldsymbol{\beta}(\mathbf{x}) = [\beta_1(\mathbf{x}), \dots, \beta_p(\mathbf{x})]^T$, and $\boldsymbol{\varepsilon}(\mathbf{x}) = [\varepsilon_1(\mathbf{x}), \varepsilon_2(\mathbf{x}), \dots, \varepsilon_N(\mathbf{x})]^T$, for every $\mathbf{x} \in \mathbb{M}_d$.

From equation (11), the second–order structure of the error term $\boldsymbol{\varepsilon} = \{\varepsilon_t, t \in \mathbb{Z}\}$ admits an infinite–dimensional matrix representation as follows:

$$\begin{aligned} \mathbf{R}_{\boldsymbol{\varepsilon}\boldsymbol{\varepsilon}} &= E[\boldsymbol{\varepsilon}(\cdot)\boldsymbol{\varepsilon}^T(\cdot)] \\ &= \begin{bmatrix} E[\varepsilon_1(\cdot) \otimes \varepsilon_1(\cdot)] & E[\varepsilon_1(\cdot) \otimes \varepsilon_2(\cdot)] & \cdots & E[\varepsilon_{t_1}(\cdot) \otimes \varepsilon_N(\cdot)] \\ E[\varepsilon_2(\cdot) \otimes \varepsilon_1(\cdot)] & E[\varepsilon_2(\cdot) \otimes \varepsilon_2(\cdot)] & \cdots & E[\varepsilon_2(\cdot) \otimes \varepsilon_N(\cdot)] \\ \vdots & \vdots & \ddots & \vdots \\ E[\varepsilon_N(\cdot) \otimes \varepsilon_1(\cdot)] & E[\varepsilon_N(\cdot) \otimes \varepsilon_2(\cdot)] & \cdots & E[\varepsilon_N(\cdot) \otimes \varepsilon_N(\cdot)] \end{bmatrix} \\ &= \begin{bmatrix} R_0 & R_1 & \cdots & R_{N-1} \\ R_1 & R_0 & \cdots & R_{N-2} \\ \vdots & \vdots & \ddots & \vdots \\ R_{N-1} & R_{N-2} & \cdots & R_0 \end{bmatrix}, \end{aligned}$$

in terms of the elements $\{R_0, R_1, \dots, R_{N-1}\}$ of the covariance operator family of the functional time series $\{\tilde{X}_t, t \in \mathbb{Z}\}$, whose values at $t = 1, \dots, N$, are here denoted as $\varepsilon_1, \dots, \varepsilon_N$. Note that the functional entries of $\mathbf{R}_{\boldsymbol{\varepsilon}\boldsymbol{\varepsilon}}$ admit the diagonal series expansion introduced in equation (3) under the conditions assumed in Theorem 4 in Ma & Malyarenko [47]. In the subsequent development we will consider the orthogonal representation of the functional regression parameters β_j , $j = 1, 2, \dots, p$, and of the observed functional values of the response variable Y_t , $t = 1, 2, \dots, N$, with respect to the orthonormal basis $\{S_{n,k}^d(\mathbf{x}), k = 1, \dots, \delta(n, d), n \in \mathbb{N}_0\}$ of eigenfunctions of the Laplace Beltrami

operator. That is, for every $j = 1, \dots, p$,

$$\beta_j(\mathbf{x}) = \sum_{n \in \mathbb{N}_0} \beta_{n,j} \sum_{k=1}^{\delta(n,d)} S_{n,k}^d(\mathbf{x}), \quad \forall \mathbf{x} \in \mathbb{M}_d. \quad (12)$$

Furthermore, under the conditions in Lemma 2, let us consider the orthogonal expansion of the observed values of the response in the basis $\{S_{n,k}^d(\mathbf{x}), k = 1, \dots, \delta(n,d), n \in \mathbb{N}_0\}$, for every $\mathbf{x} \in \mathbb{M}_d$, and for each $t \in \mathbb{Z}$,

$$Y_t(\mathbf{x}) = \sum_{j=1}^p \sum_{n \in \mathbb{N}_0} \sum_{k=1}^{\delta(n,d)} Y_{n,k}(t) S_{n,k}^d(\mathbf{x}) = \sum_{j=1}^p \sum_{n \in \mathbb{N}_0} \sum_{k=1}^{\delta(n,d)} [X_{t,j} \beta_{n,j} + V_{n,k}(t)] S_{n,k}^d(\mathbf{x}), \quad (13)$$

where convergence holds pointwise on \mathbb{M}_d in the mean-square sense for each fixed $t = 1, \dots, N$, and in the space $\mathcal{L}_{\tilde{H}}^2(\Omega, \mathcal{A}, P) = L^2(\Omega \times \mathbb{M}_d \times [0, N], P(d\omega) \otimes d\nu \otimes dt)$, under conditions of Lemma 2.

3.1 GLS functional parameter estimation

The $[L^2(\mathbb{M}_d, d\nu, \mathbb{R})]^p$ -valued GLS functional parameter estimator of $\boldsymbol{\beta} = [\beta_1, \beta_2, \dots, \beta_p]^T$ is computed from projection into the orthonormal basis $\{S_{n,k}^d, k = 1, \dots, \delta(n,d), n \in \mathbb{N}_0\}$ of eigenfunctions of the Laplace Beltrami operator Δ_d on $L^2(\mathbb{M}_d, d\nu, \mathbb{R})$, in the spirit of the approach adopted in Ruiz-Medina [59]. Specifically, for each $n \in \mathbb{N}_0$, one can define the matrix

$$\mathbf{\Lambda}_n = \begin{bmatrix} B_n(0) & \cdots & B_n(N-1) \\ \vdots & \ddots & \vdots \\ B_n(N-1) & \cdots & B_n(0) \end{bmatrix},$$

and the respective vector response and error term projections

$$\mathbf{Y}_n = [Y_n(1), Y_n(2), \dots, Y_n(N)]^T \text{ and } \boldsymbol{\varepsilon}_n = [V_n(1), V_n(2), \dots, V_n(N)]^T$$

with $\mathbf{n} = (n_1, \dots, n_{\delta(n,d)})$, into the eigenspace \mathcal{H}_n of the Laplace Beltrami operator, as well as the corresponding vector of projections $\boldsymbol{\beta}_n = [\beta_{n,1}, \dots, \beta_{n,p}]^T$ of the functional regression parameter.

Hence, the minimizer $\hat{\boldsymbol{\beta}}$ of the mean quadratic loss function L , given by

$$\begin{aligned} L &= \|\mathbf{Y} - \mathbf{X}\boldsymbol{\beta}\|_{\mathbf{R}\boldsymbol{\varepsilon}\boldsymbol{\varepsilon}^{-1}} = \sum_{n \in \mathbb{N}_0} [\mathbf{Y}_n - \mathbf{X}\boldsymbol{\beta}_n]^T \mathbf{\Lambda}_n^{-1} [\mathbf{Y}_n - \mathbf{X}\boldsymbol{\beta}_n] \\ &= \sum_{n \in \mathbb{N}_0} \|\boldsymbol{\varepsilon}_n\|_{\mathbf{\Lambda}_n^{-1}}^2, \end{aligned} \quad (14)$$

has Fourier coefficients $\widehat{\boldsymbol{\beta}}_n$ defined as

$$\widehat{\boldsymbol{\beta}}_n = \left[\widehat{\beta}_{n,1}, \widehat{\beta}_{n,2}, \dots, \widehat{\beta}_{n,p} \right]^T = (\mathbf{X}^T \boldsymbol{\Lambda}_n^{-1} \mathbf{X})^{-1} \mathbf{X}^T \boldsymbol{\Lambda}_n^{-1} \mathbf{Y}_n, \quad n \in \mathbb{N}_0. \quad (15)$$

Thus, the theoretical predictor is defined by

$$\widehat{\mathbf{Y}} = \mathbf{X} \widehat{\boldsymbol{\beta}} \quad (16)$$

3.2 Distributional characteristics of GLS estimator

For every $n \in \mathbb{N}_0$, $\widehat{\boldsymbol{\beta}}_n$ is an unbiased estimator of $\boldsymbol{\beta}_n$ since

$$\begin{aligned} E \left[\widehat{\boldsymbol{\beta}}_n \right] &= E \left[(\mathbf{X}^T \boldsymbol{\Lambda}_n^{-1} \mathbf{X})^{-1} \mathbf{X}^T \boldsymbol{\Lambda}_n^{-1} \mathbf{Y}_n \right] \\ &= (\mathbf{X}^T \boldsymbol{\Lambda}_n^{-1} \mathbf{X})^{-1} \mathbf{X}^T \boldsymbol{\Lambda}_n^{-1} E \left[\mathbf{Y}_n \right] \\ &= (\mathbf{X}^T \boldsymbol{\Lambda}_n^{-1} \mathbf{X})^{-1} \mathbf{X}^T \boldsymbol{\Lambda}_n^{-1} \mathbf{X} \boldsymbol{\beta}_n \\ &= \boldsymbol{\beta}_n. \end{aligned} \quad (17)$$

Hence, from (17), for every $\mathbf{x} \in \mathbb{M}_d$,

$$\begin{aligned} E \left[\widehat{\boldsymbol{\beta}}(\mathbf{x}) \right] &= E \left[\left(\sum_{n=0}^{\infty} \widehat{\beta}_{n,1} \sum_{k=1}^{\delta(n,d)} S_{n,k}^d(\mathbf{x}), \dots, \sum_{n=0}^{\infty} \widehat{\beta}_{n,p} \sum_{k=1}^{\delta(n,d)} S_{n,k}^d(\mathbf{x}) \right)^T \right] \\ &= \left(\sum_{n=0}^{\infty} E \left[\widehat{\beta}_{n,1} \right] \sum_{k=1}^{\delta(n,d)} S_{n,k}^d(\mathbf{x}), \dots, \sum_{n=0}^{\infty} E \left[\widehat{\beta}_{n,p} \right] \sum_{k=1}^{\delta(n,d)} S_{n,k}^d(\mathbf{x}) \right)^T \\ &= \left(\sum_{n=0}^{\infty} \beta_{n,1} \sum_{k=1}^{\delta(n,d)} S_{n,k}^d(\mathbf{x}), \dots, \sum_{n=0}^{\infty} \beta_{n,p} \sum_{k=1}^{\delta(n,d)} S_{n,k}^d(\mathbf{x}) \right)^T \\ &= \boldsymbol{\beta}(\mathbf{x}). \end{aligned}$$

Finally, as it is well known, since for every $n \in \mathbb{N}_0$,

$$\widehat{\boldsymbol{\beta}}_n = \boldsymbol{\beta}_n + (\mathbf{X}^T \boldsymbol{\Lambda}_n^{-1} \mathbf{X})^{-1} \mathbf{X}^T \boldsymbol{\Lambda}_n^{-1} \boldsymbol{\varepsilon}_n, \quad (18)$$

we have

$$\begin{aligned} \text{Var} \left[\widehat{\boldsymbol{\beta}}_n \right] &= E \left[\left(\widehat{\boldsymbol{\beta}}_n - \boldsymbol{\beta}_n \right)^T \left(\widehat{\boldsymbol{\beta}}_n - \boldsymbol{\beta}_n \right) \right] \\ &= (\mathbf{X}^T \boldsymbol{\Lambda}_n^{-1} \mathbf{X})^{-1} \mathbf{X}^T \boldsymbol{\Lambda}_n^{-1} \boldsymbol{\Lambda}_n \boldsymbol{\Lambda}_n^{-1} \mathbf{X} (\mathbf{X}^T \boldsymbol{\Lambda}_n^{-1} \mathbf{X})^{-1} \\ &= (\mathbf{X}^T \boldsymbol{\Lambda}_n^{-1} \mathbf{X})^{-1}. \end{aligned} \quad (19)$$

3.3 Functional spectral based plug-in estimation of the functional regression parameter

This section presents a plug-in GLS estimation methodology when the second order structure of the error term is unknown. In our case, the entries of the matrix sequence $\{\mathbf{\Lambda}_n, n \in \mathbb{N}_0\}$ are misspecified. The approach presented is based on the estimation of such entries in the spectral domain by minimum contrast, under a semiparametric modelling framework, applying the methodology introduced in Ovalle–Muñoz & Ruiz–Medina [53], and Ruiz–Medina [60]. Specifically, we will assume that the function elements of the Fourier transform sequence

$$f_{n,\theta}(\omega) = \int_{-\pi}^{\pi} \exp(-i\omega t) \widehat{B}_{n,\theta}(t) dt, \quad \omega \in [-\pi, \pi], \quad n \in \mathbb{N}_0,$$

admit the following semiparametric modelling: For every $n \in \mathbb{N}_0$,

$$f_{n,\theta}(\omega) = B_n^\eta(0) M_n(\omega) [4(\sin(\omega/2))^2]^{-\alpha(n,\theta)/2}, \quad \theta \in \Theta, \quad \omega \in [-\pi, \pi], \quad (20)$$

where $\alpha(n, \theta)$, $M_n(\omega)$, and $B_n^\eta(0)$ are the eigenvalues of the LRD operator \mathcal{A}_θ , of the Short Range Dependence (SRD) spectral family $\{\mathcal{M}_\omega, \omega \in [-\pi, \pi]\}$, and of the autocovariance operator R_0^η of the manifold white noise innovation process η involved in the definition of the error term ε , respectively. Hence, the elements of the spectral density operator family $\{\mathcal{F}_{\omega,\theta}, \omega \in [-\pi, \pi]\}$ introduced in equation (8) are respectively approximated by

$$\left\{ \mathcal{F}_{\omega, \widehat{\theta}_N}, \omega \in [-\pi, \pi] \right\},$$

with $\widehat{\theta}_N$ denoting the minimum contrast estimator of parameter θ based on a functional sample of size N (see equations (3.8)–(3.16) in Ovalle–Muñoz & Ruiz–Medina [53], or equations (5.1)–(5.19) in Ruiz–Medina [60]). Fourier transform inversion formula

$$\widehat{B}_{n, \widehat{\theta}_N}(t) = \int_{-\pi}^{\pi} \exp(i\omega t) f_{n, \widehat{\theta}_N}(\omega) d\omega, \quad n \in \mathbb{N}_0,$$

is then applied to obtain the estimated matrix sequence

$$\widehat{\mathbf{\Lambda}}_{n, \widehat{\theta}_N} = \left(\begin{bmatrix} \widehat{B}_{n, \widehat{\theta}_N}(0) & \cdots & \widehat{B}_{n, \widehat{\theta}_N}(N-1) \\ \vdots & \ddots & \vdots \\ \widehat{B}_{n, \widehat{\theta}_N}(N-1) & \cdots & \widehat{B}_{n, \widehat{\theta}_N}(0) \end{bmatrix} \right), \quad n \in \mathbb{N}_0.$$

The plug-in GLS estimators of the Fourier coefficients of the functional multiple regression vector parameter β , with respect to the orthonormal basis of eigenfunctions of the Laplace Beltrami operator, admit the following expression:

$$\widehat{\beta}_{n,\widehat{\theta}_N} = \left(\mathbf{X}^T \widehat{\Lambda}_{n,\widehat{\theta}_N}^{-1} \mathbf{X} \right)^{-1} \mathbf{X}^T \widehat{\Lambda}_{n,\widehat{\theta}_N}^{-1} \mathbf{Y}_n, \quad n \in \mathbb{N}_0,$$

and the corresponding plug-in predictor is then computed as

$$\widehat{\mathbf{Y}}_{n,\widehat{\theta}_N} = \mathbf{X} \widehat{\beta}_{n,\widehat{\theta}_N}. \quad (21)$$

4 Asymptotic properties of the GLS functional parameter estimator

Model (10) can be interpreted as a particular case of the multiple functional regression model introduced in equation (1) in Ruiz-Medina, Miranda & Espejo [61], when the Hilbert space $H = L^2(\mathbb{M}_d, d\nu, \mathbb{R})$ is considered. Specifically, the functional regression model (10) can be isometrically identified with multiple functional regression model in equation (1) in Ruiz-Medina, Miranda & Espejo [61], in the special case of diagonal kernel regressors with one non-null coefficient or eigenvalue.

Theorem 1 in Ruiz-Medina, Miranda & Espejo [61] provides the conditions for the asymptotic normality of the GLS $\widehat{\beta}$ estimator of the vector functional regression parameter β , in the case where the second-order structure of the functional error term ε is known. In our case, when the function sequence $\{f_n(\omega), \omega \in [-\pi, \pi], n \in \mathbb{N}_0\}$ is totally specified, and characterizes the pure point spectra of the elements of the spectral density operator family $\{\mathcal{F}_\omega, \omega \in [-\pi, \pi]\}$ of the error term. Furthermore, in this case, Assumptions A1–A6 in Ruiz-Medina, Miranda & Espejo [61] ensure the strong-consistency of the GLS estimator $\widehat{\beta}$ of β , as given in their Theorem 2. Finally, under Assumptions $\widetilde{A}5 - \widetilde{A}6$ in Ruiz-Medina, Miranda & Espejo [61], in the case of unknown $\{f_n(\omega), \omega \in [-\pi, \pi], n \in \mathbb{N}_0\}$ sequence, Proposition 1 in Ruiz-Medina, Miranda & Espejo, [61], adapted to our time-varying finite-dimensional design matrix \mathbf{X} , provides the strong-consistency, in the norm of the space $[L^2(\mathbb{M}_d, d\nu, \mathbb{R})]^p$, of the ordinary least-squares estimator of the functional regression parameter β . From Theorem 2 in Ruiz-Medina [60] (see also Theorem 2 in Ovalle-Muñoz & Ruiz-Medina [53]), applying Fourier transform inversion formula, the consistency in the sense of the integrated weighted mean square error, measured in the norm of the space of Hilbert-Schmidt operators $\mathcal{S}(L^2(\mathbb{M}_d, d\nu, \mathbb{C}))$ on $L^2(\mathbb{M}_d, d\nu, \mathbb{C})$, of the plug-in GLS estimator of β follows. Hence, the weak-consistency of the plug-in GLS estimator of β in the norm of $\mathcal{S}(L^2(\mathbb{M}_d, d\nu, \mathbb{C}))$ also holds.

5 Simulation study

The simulation study undertaken in this section illustrates the sample properties of the theoretical and plug-in functional response predictors introduced in equations (16) and (21), respectively. The numerical results are displayed under misspecified, and totally specified model of the functional error term. Specifically, the projected (into the basis of eigenfunctions of the Laplace Beltrami operator) empirical mean-quadratic and absolute errors are computed. Their empirical distributional characteristics are visualized in terms of their histograms. Thus, at each eigenspace of the Laplace Beltrami operator, the projected residuals are analyzed, under decreasing and increasing sequence of the eigenvalues of the LRD operator \mathcal{A}_θ in equation (20). All the numerical results are displayed for $\mathbb{M}_d = \mathbb{S}_2 = \{\mathbf{x} \in \mathbb{R}^3 : \|\mathbf{x}\| = 1\}$, and, hence, for $H = L^2(\mathbb{S}_2, d\nu, \mathbb{R})$, and its complex version $L^2(\mathbb{S}_2, d\nu, \mathbb{C})$.

Note that the proposed methodology in Section 3 does not suppose a specific structure regarding the scalar time-varying entries in the design matrix \mathbf{X} . In our simulation study, we adopt the framework of one way ANOVA, assuming the application of five treatments through time, respectively leading to five functional response spherical means, $\beta_j(\mathbf{x})$, $\mathbf{x} \in \mathbb{S}_2$, $j = 1, 2, \dots, p$. This example can be interpreted in the field of change point analysis, since one can adopt this framework to detecting changes through time in the spherical trend of the observed functional time series (see, e.g., Dette & Quanz [25]).

In the model generations, truncation at discrete Legendre frequency $M = 30$ has been achieved. The corresponding Fourier coefficients of the $L^2(\mathbb{S}_2, d\nu, \mathbb{R})$ -valued parameters β_j , $j = 1, 2, \dots, p$, with respect the orthonormal basis of eigenfunctions of the Laplace Beltrami operator, are given by:

$$\begin{aligned} \beta_{n,j} &= \frac{1}{6} \frac{x_n^{\alpha-1} (1-x_n)^{\varrho_j-1} \Gamma(\alpha + \varrho_j)}{\Gamma(\alpha) \Gamma(\varrho_j)}, \quad \alpha, \varrho_j > 0 & (22) \\ \alpha &= 2, \quad \varrho_j = \frac{5j}{j+1}, \quad j = 1, 2, \dots, p, \quad p = 5 \\ x_1 &= 0, \quad x_n = x_{n-1} + \frac{1}{30-1}, \quad n = 2, 3, \dots, 30. \end{aligned}$$

These Fourier coefficients are displayed in Figure 1. The projected regression parameters into the direct sum $\bigoplus_{n=1}^{30} \mathcal{H}_n$ of the eigenspaces \mathcal{H}_n , $n = 1, \dots, 30$, of the Laplace Beltrami operator can also be seen in Figure 2.

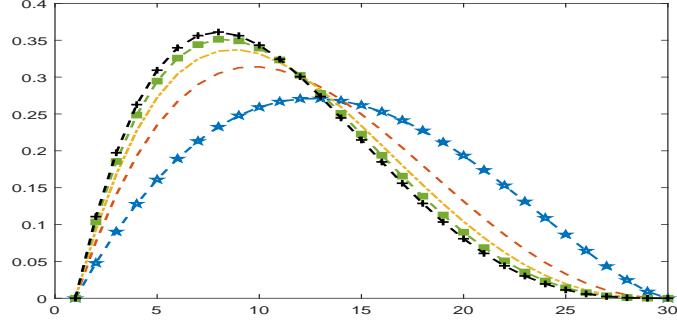


Figure 1: Fourier coefficients $\beta_{n,j}$, $n = 1, 2, \dots, 30$, for $j = 1, 2, 3, 4, 5$, are respectively displayed in blue star-dashed line, red dashed line, orange dotted line, green squares-dashed line and black cross-dashed line.

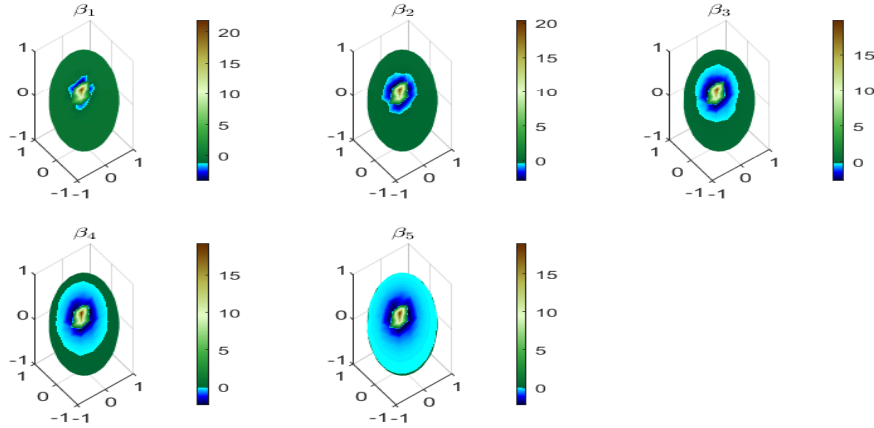


Figure 2: The regression parameters $\beta_j(\mathbf{x})$, $\mathbf{x} \in \mathbb{S}_2$, $j = 1, 2, \dots, 5$, projected into the direct sum of eigenspaces \mathcal{H}_n , $n = 1, 2, \dots, 30$, of the Laplace Beltrami operator on $L^2(\mathbb{S}_2, d\nu, \mathbb{R})$.

In this simulation study, we have considered the case where the error term $\varepsilon = \{\varepsilon_t, t \in \mathbb{Z}\}$ obeys a multifractionally integrated SPHARMA(1, 1) equation. Equivalently, the following state equation characterizes the behavior of ε : For each $t \in \mathbb{Z}$,

$$(\mathcal{I}_{L^2(\mathbb{S}_2, d\nu, \mathbb{R})} - B)^{A_{\theta_0}/2}(\Phi_p(B)\varepsilon_t)(\mathbf{x}) = \eta_t(\mathbf{x}) + (\Psi_q(B)\eta_t)(\mathbf{x}), \quad \mathbf{x} \in \mathbb{S}_2,$$

where \mathcal{A}_{θ_0} denotes the LRD integral operator with isotropic kernel $\mathcal{K}_{\mathcal{A}_{\theta_0}}$ satisfying

$$\mathcal{K}_{\mathcal{A}_{\theta_0}}(\mathbf{x}, \mathbf{y}) = \sum_{n \in \mathbb{N}_0} \alpha(n, \theta_0) \sum_{j=1}^{\delta(n,d)} S_{n,j}^d(\mathbf{x}) S_{n,j}^d(\mathbf{y}), \quad \mathbf{x}, \mathbf{y} \in \mathbb{S}_2,$$

with, as before, $d = 2$, $\delta(n, d) = \delta(n, 2) = 2n + 1$. We have considered $l_\alpha(\theta_0) \leq \alpha(n, \theta_0) \leq L_\alpha(\theta_0)$, with $l_\alpha(\theta_0), L_\alpha(\theta_0) \in (0, 1/2)$. $L^2(\mathbb{S}_2, d\nu, \mathbb{R})$ -valued strong white noise process $\eta = \{\eta_t(\mathbf{x}), \mathbf{x} \in \mathbb{S}_2, t \in \mathbb{Z}\}$ has variance $\sigma_\eta^2 = \sum_{n \in \mathbb{N}_0} \sigma_n^2$. Furthermore, $\Phi_p(B) = 1 - \sum_{k=1}^p \Phi_k B^k$, and $\Psi_q(B) = \sum_{l=1}^q \Psi_l B^l$ respectively denote the autoregressive and moving average polynomial operators, with $\Phi_k, k = 1, 2, \dots, p$ and $\Psi_l, l = 1, 2, \dots, q$ being invariant positive self-adjoint bounded operators on $L^2(\mathbb{S}_2, d\nu, \mathbb{R})$. Each one of the above operators admits the diagonal series expansion:

$$\begin{aligned} \Phi_k &= \sum_{n \in \mathbb{N}_0} \lambda_n(\Phi_k) \sum_{j=1}^{\delta(n,d)} S_{n,j}^d \otimes S_{n,j}^d, \quad k = 1, \dots, p \\ \Psi_l &= \sum_{n \in \mathbb{N}_0} \lambda_n(\Psi_l) \sum_{j=1}^{\delta(n,d)} S_{n,j}^d \otimes S_{n,j}^d, \quad l = 1, \dots, q. \end{aligned}$$

The results displayed correspond to the generation of functional samples of size $N = 50, 100, 500$ of the multifractionally integrated SPHARMA(1,1) process defining the error term in our regression model. In particular, the following parameter values have been considered in the generations of SPHARMA(1,1) process : $\sigma_n^2 = (n+1)^{-3/2}$, $\lambda_n(\Phi_k) = [0.7(n + \frac{1}{n})]^{-3/2}$, $\lambda_n(\Psi_l) = 0.4(n + \frac{1}{n})^{-3/2}$, $n = 1, 2, \dots, 30$, $k = l = 1$. Multifractionally integration has been achieved in the spectral domain in terms of the following parameterized eigenvalues $\{\alpha(n, \theta_0), n \in$

$\mathbb{N}_0\}$ of the LRD operator \mathcal{A}_{θ_0} :

$$\alpha(n, \theta_0) = \frac{\theta_{0,1}x_n^2 + \theta_{0,2}x_n + \theta_{0,3}}{\theta_{0,4}}, \theta_0 = (\theta_{0,1}, \theta_{0,2}, \theta_{0,3}, \theta_{0,4}), \quad (23)$$

$$\theta_{0,1} = 0.75, \theta_{0,2} = 0.76, \theta_{0,3} = 0.77,$$

$$\theta_{0,4} = \sup_{i=1,2,\dots,100} f(x_n, i),$$

$$f(x_n, i) = \frac{1}{100} (ix_n^2 + (i+1)x_n + (i+2)),$$

$$x_1 = 0, x_n = x_{n-1} + \frac{30}{29}, n = 2, 3, \dots, 30,$$

$$\alpha(n, v_0) = 1 - \frac{1}{9 \exp(v_{0,1} + v_{0,2}x_n)}, v_0 = (v_{0,1}, v_{0,2}) = (1, 1), \quad (24)$$

$$x_1 = -\pi, x_n = x_{n-1} + \frac{2\pi}{30-1}, n = 2, 3, \dots, 30,$$

where we have considered a Decreasing Positive Bounded Sequence (DPBS) and an Increasing Positive Bounded Sequence (IPBS) of eigenvalues $\{\alpha(n, \theta_0), n \in \mathbb{N}_0\}$ and $\{\alpha(n, v_0), n \in \mathbb{N}_0\}$ of the LRD operator, respectively defined in equations (23) and (24) (see also Figure 3).

The values $l_\alpha = 1.0192$ and $L_\alpha = 0.2699$ have been considered in DPBS, and $l_\alpha = 0.0541$ and $L_\alpha = 0.9982$ in IPBS of eigenvalues of the LRD operator. Note that the dominant eigenspace of the Laplace Beltrami operator where the largest dependence range in time is displayed by the projected error term under the DPBS corresponds to the first eigenspace plotted, while, in the IPBS case, the projected process displays the strongest LRD in the last eigenspace of the Laplace Beltrami operator plotted in Figure 3.

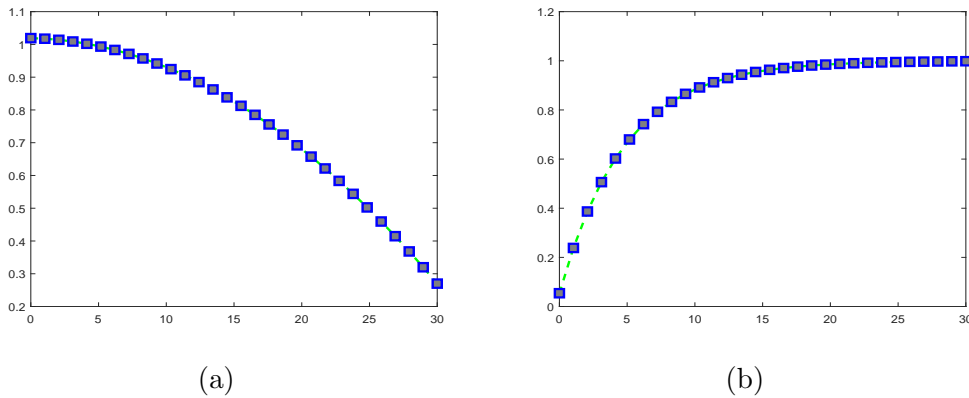


Figure 3: The first 30 eigenvalues $\alpha(n, \theta_0), n = 1, \dots, 30$, of the LRD operator \mathcal{A}_{θ_0} . The considered DPBS of eigenvalues is plotted at the left-hand side, and the IPBS of eigenvalues is plotted at the right hand-side.

5.1 Spherical multiscale residual analysis under totally specified model

The generations displayed in Figures 4 and 5 correspond to the case of a DPBS of eigenvalues of the LRD operator. Specifically, the empirical mean of the response (REM), based on $R = 100$ repetitions of a functional sample of size $N = 500$, projected into the direct sum $\bigoplus_{n=1}^{30} \mathcal{H}_n$ of the eigenspaces \mathcal{H}_n , $n = 1, \dots, 30$, of the Laplace Beltrami operator is showed in Figure 4 at times $t = 0, 62, 124, 187, 249, 311, 374, 436, 499$. The empirical mean (RT-PEM) (based on the same $R = 100$ repetitions) of the theoretical predictor, projected into the direct sum $\bigoplus_{n=1}^{30} \mathcal{H}_n$, is shown in Figure 5 at times $t = 0, 62, 124, 187, 249, 311, 374, 436, 499$.

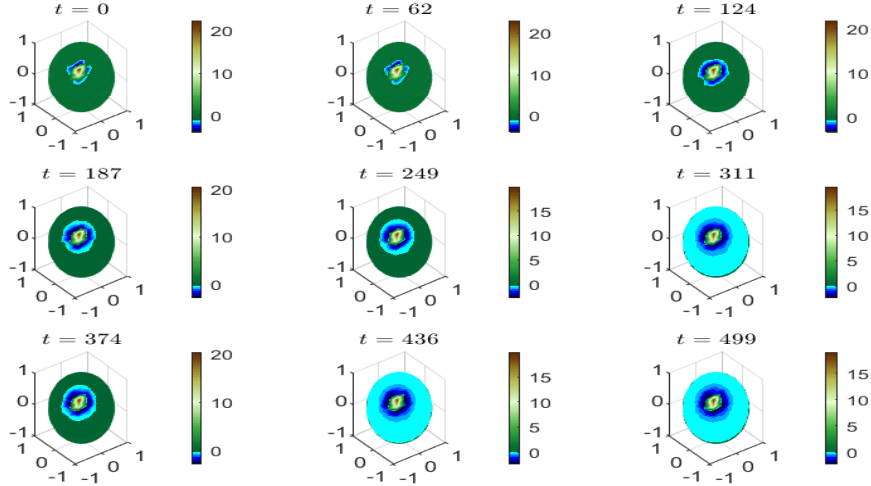


Figure 4: REM $\hat{E}[Y_t(\mathbf{x})]$, $\mathbf{x} \in \mathbb{S}_2$, based on $R = 100$ repetitions, at times $t = 0, 62, 124, 187, 249, 311, 374, 436, 499$, projected into the direct sum of the eigenspaces \mathcal{H}_n , $n = 1, 2, \dots, 30$ of the Laplace Beltrami operator on $L^2(\mathbb{S}_2, d\nu, \mathbb{R})$, under DPBS of eigenvalues of LRD operator. The functional sample size generated is $T = 500$.

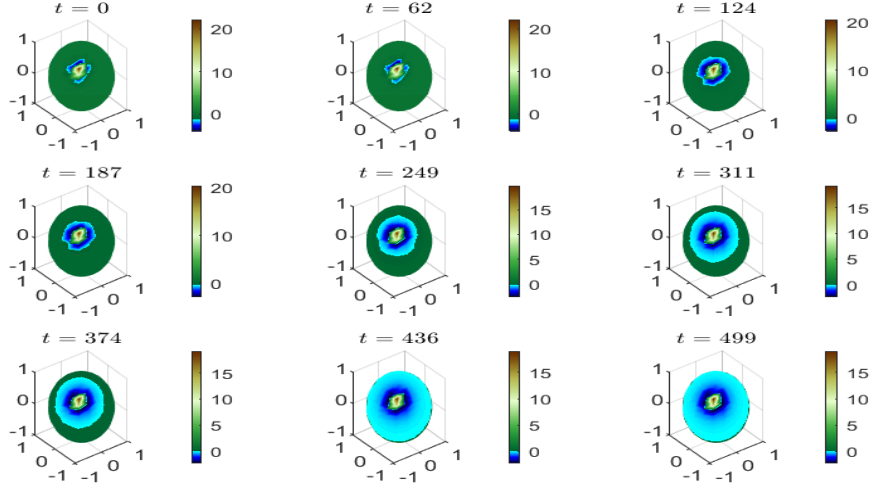


Figure 5: RTPEM $\hat{E} [\hat{Y}_t(\mathbf{x})]$, $\mathbf{x} \in \mathbb{S}_2$, based on $R = 100$ repetitions, at times $t = 0, 62, 124, 187, 249, 311, 374, 436, 499$, projected into the direct sum of the eigenspaces \mathcal{H}_n , $n = 1, 2, \dots, 30$ of the Laplace Beltrami operator on $L^2(\mathbb{S}_2, d\nu, \mathbb{R})$, under DPBS of eigenvalues of LRD operator. The functional sample size generated is $T = 500$.

Figure 6 illustrates unbiasedness of $\hat{\beta}_j(\mathbf{x})$, $\mathbf{x} \in \mathbb{S}_2$, $j = 1, 2, 3, 4, 5$, whose empirical means based on $R = 100$ repetitions under DPBS of eigenvalues of LRD operator are plotted in this figure for functional sample sizes $N = 50, 100, 500$. The slow temporal decay of time-varying eigenvalue $B_n(t)$ as t increases acts as a regularizer, regarding the singular behavior of the linear filter defining the GLS parameter estimator in (15) as n increases for a fixed time t . Note that this singular behavior is induced by Λ_n^{-1} as n increases due to the fast decay of the pure point spectra of the elements of the trace covariance operator family. This regularization effect, which becomes stronger when the functional sample size increases, can be observed at least up to discrete Legendre frequency $n = M = 30$, being more pronounced at low and high discrete Legendre frequencies under DPBS and IPBS of eigenvalues of the LRD operator, respectively. Thus, the highest empirical mean quadratic errors are observed at spherical scales corresponding to intermediate Legendre frequencies $n \in [10, 20]$ (see, Figures 7 and 8).

The incorporation of the time-varying coefficients defined by the entries of the design matrix leads to the definition of the theoretical predictor in equation (16). The temporal pointwise values of the functional Empirical Mean Quadratic Errors (EMQEs), based on $R = 100$ repetitions, associated with the theoretical response predictor reflect the effect of the spherical-scale-varying strong-dependence in

time displayed by the response. Hence, the same conclusions follow as in the GLS parameter estimator (see Figure 9). Note that, in the analysis performed in terms of the empirical distribution of the L^1 norms of the response prediction errors at each eigenspace \mathcal{H}_n of the Laplace Beltrami operator, for $n = 1, \dots, 30$, a slighter LRD effect is observed in all spherical scales analyzed under DPBS than under IPBS of eigenvalues of the LRD operator, as one can observe from the supports and modes of the empirical distributions plotted for the functional sample sizes $N = 50, 100, 500$ in Figures 10 and 11.

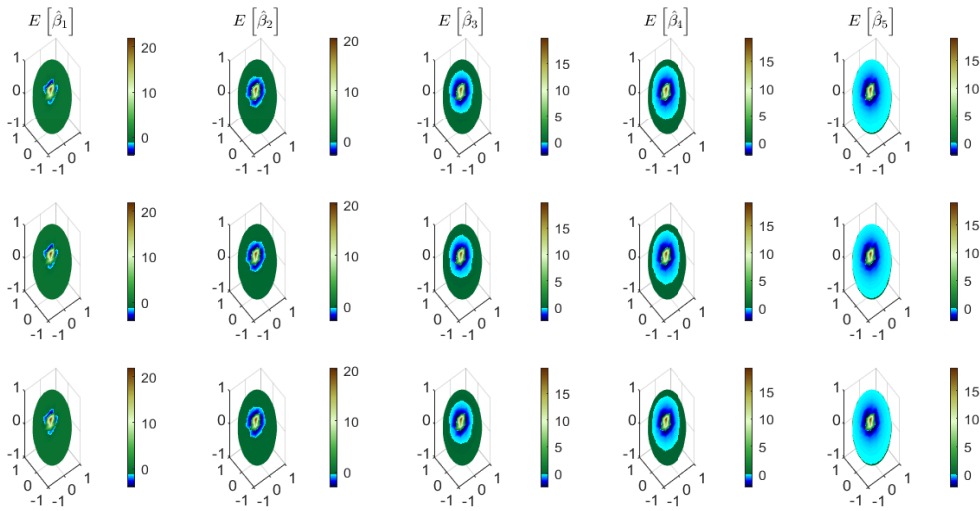


Figure 6: Under DPBS of eigenvalues of the LRD operator, the projected empirical mean $\hat{E} [\hat{\beta}_j(\mathbf{x})]$, $\mathbf{x} \in \mathbb{S}_2$, of the computed values of the GLS parameter estimator, based on $R = 100$ repetitions, are showed for $j = 1, 2, 3, 4, 5$. The results for functional sample sizes $N = 50, 100, 500$ are respectively presented by rows.

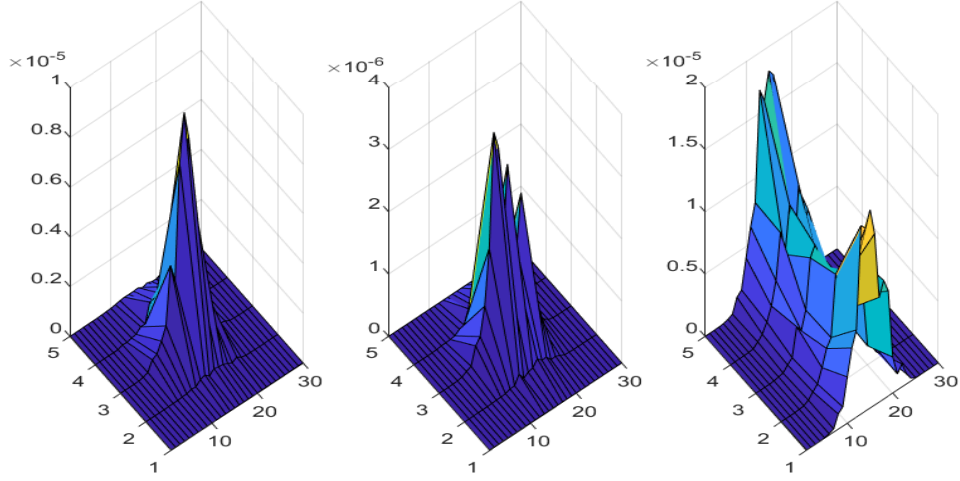


Figure 7: Under DPBS of eigenvalues of the LRD operator, the Empirical Mean Quadratic Errors (EMQEs) $\hat{E} \left[(\hat{\beta}_{n,j} - \beta_{n,j})^2 \right], n = 1, 2, \dots, 30, j = 1, 2, \dots, 5$, based on $R = 100$ repetitions, for functional sample sizes $N = 50, 100, 500$ are respectively plotted from the left-hand-side to the right-hand-side.

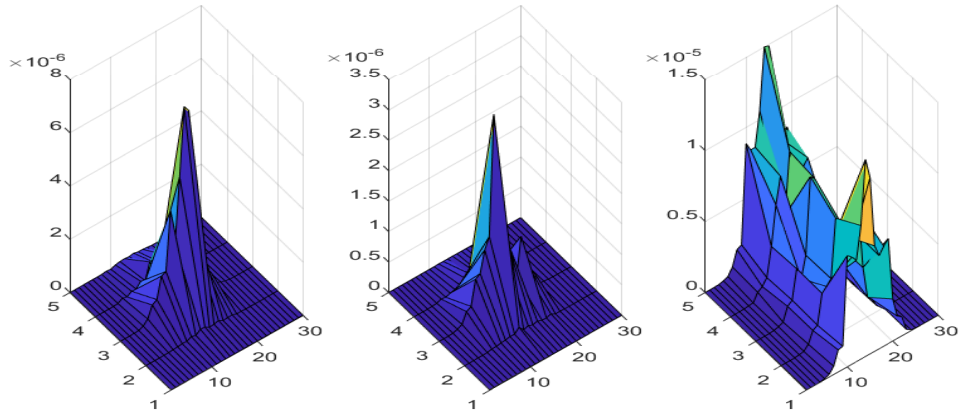


Figure 8: Under IPBS of eigenvalues of the LRD operator, the EMQEs $\hat{E} \left[(\hat{\beta}_{n,j} - \beta_{n,j})^2 \right], n = 1, 2, \dots, 30, j = 1, 2, \dots, 5$, based on $R = 100$ repetitions, for functional sample sizes $N = 50, 100, 500$ are respectively plotted from the left-hand-side to the right-hand-side.

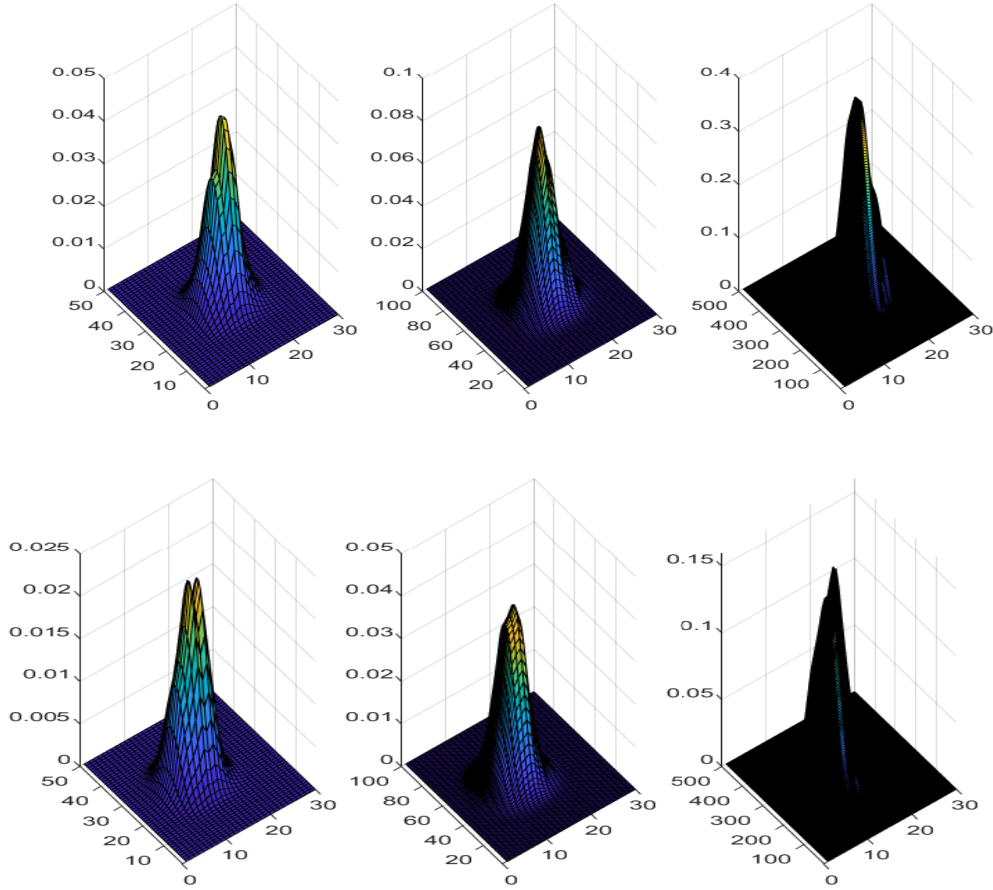


Figure 9: Projected EMQEs of the theoretical predictor projections $\widehat{E} \left[(\widehat{Y}_{\mathbf{n}}(t) - Y_{\mathbf{n}}(t))^2 \right]$, into 30 eigenspaces of the Laplace Beltrami operator, for $t = 1, 2, \dots, N$, based on $R = 100$ repetitions, for functional sample sizes $N = 50, 100, 500$ from the left-hand-side to the right-hand-side, respectively, under the IPBS (at the top), and under DPBS (at the bottom) of eigenvalues of the LRD operator.

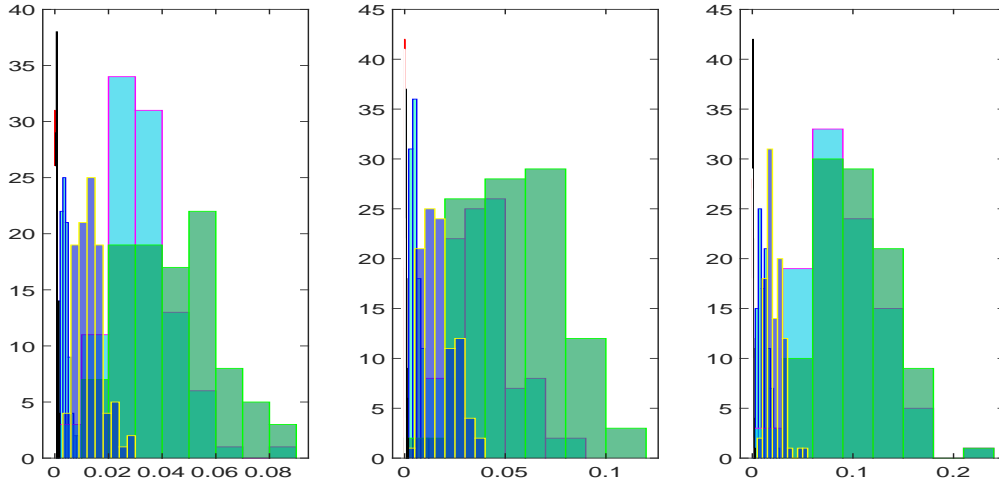


Figure 10: Empirical distribution, based on $R = 100$ repetitions, of $\|\tilde{Y}_{\mathbf{n}}(t) - Y_{\mathbf{n}}(t)\|_{L^1([1,N])}$, for projections into Laplace–Beltrami eigenspaces \mathcal{H}_n , $n = 1, 5, 10, 15, 20, 25, 30$, for functional sample sizes $T = 50, 100, 500$ from the left–hand side to the right–hand side, respectively, under the DPBS of eigenvalues of the LRD operator.

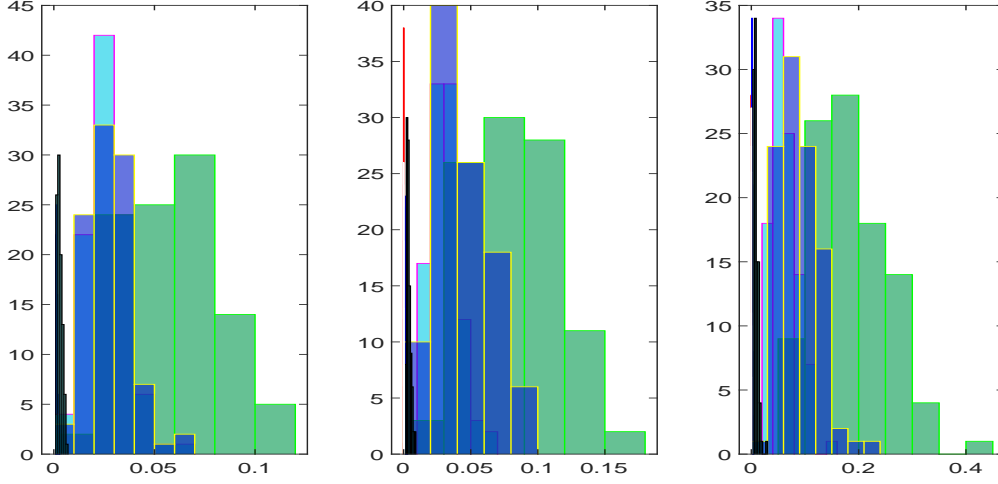


Figure 11: Empirical distribution, based on $R = 100$ repetitions, of $\|\hat{Y}_n(t) - Y_n(t)\|_{L^1([1,N])}$, for projections into Laplace–Beltrami eigenspaces \mathcal{H}_n , $n = 1, 5, 10, 15, 20, 25, 30$, for functional sample sizes $T = 50, 100, 500$ from the left–hand side to the right–hand side, respectively, under the IPBS of eigenvalues of the LRD operator.

5.2 Results under misspecified model

The numerical results displayed in this section are obtained from the plug–in estimation of β , based on the minimum contrast estimation of the parameterized frequency–varying eigenvalues of the elements of the spectral density operator family, as given in Section 3.3. Figures 12 and 13 display the empirical distribution of the L^1 –norm, based on $R = 100$ repetitions, of the empirical absolute functional errors, associated with minimum contrast estimation from the generated functional samples of sizes $N = 50, 100, 500$.

The resulting spherical scale dependent EMQEs, associated with the plug–in estimation of the Fourier coefficients of the functional regression parameter vector β from its projection into the eigenspaces \mathcal{H}_n , $n = 1, \dots, 30$, of the Laplace Beltrami operator are then computed (see Figures 14 and 15). The corresponding temporal pointwise values of the response prediction EMQEs are also displayed by spherical scales (corresponding to projection into \mathcal{H}_n , $n = 1, \dots, 30$,) for functional sample sizes $N = 50, 100, 500$, based on $R = 100$ repetitions (see Figures 16 and 17). All the above numerical results are visualized under DPBS and IPBS of eigenvalues of the LRD operator.

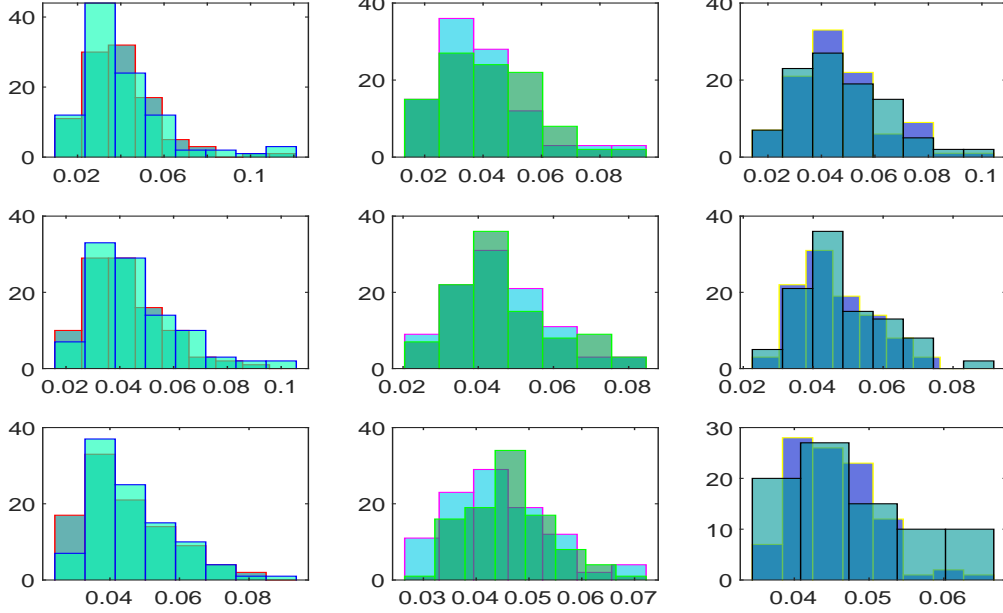


Figure 12: Under DPBS of eigenvalues of the LRD operator, the empirical distribution, based on $R = 100$ repetitions, of $\|f_{n,\hat{\theta}_N}(\cdot) - f_{n,\theta_0}(\cdot)\|_{L^1([-\pi,\pi])}$ is showed. The results are displayed for projections into \mathcal{H}_n , for $n = 5 - 10$ at the left hand-side, for $n = 15 - 20$ at the center, and for $n = 25 - 30$ at the right-hand side. By rows, the empirical distributions plotted correspond to the functional sample sizes $N = 50$ (first row), $N = 100$ (second row) and $N = 500$ (third row).

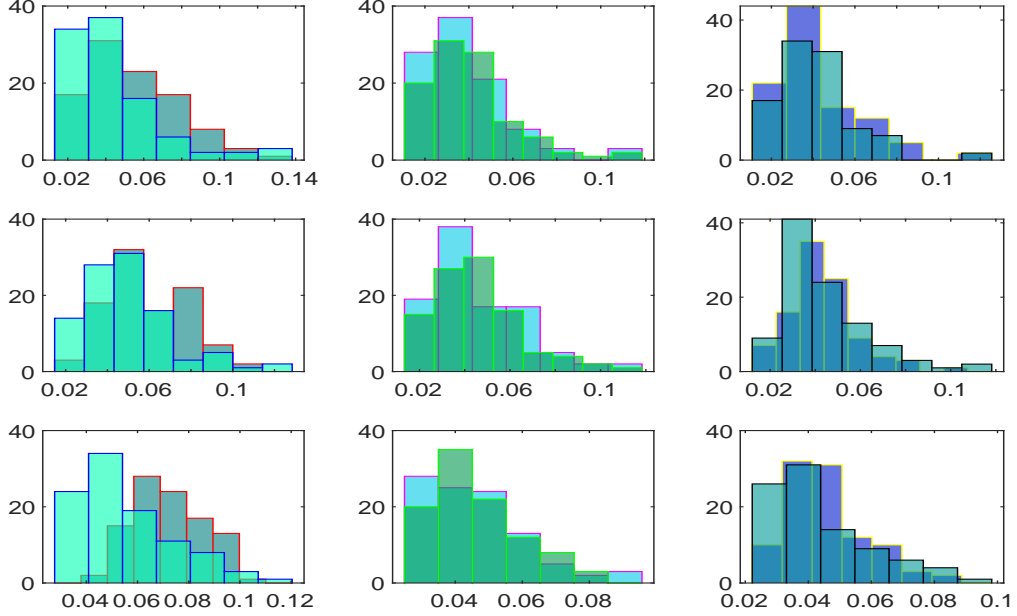


Figure 13: Under IPBS of eigenvalues of the LRD operator, the empirical distribution, based on $R = 100$ repetitions, of $\|f_{n,\hat{\theta}_N}(\cdot) - f_{n,\theta_0}(\cdot)\|_{L^1([-\pi,\pi])}$ is showed. The results are displayed for projections into \mathcal{H}_n , for $n = 5 - 10$ at the left hand-side, for $n = 15 - 20$ at the center, and for $n = 25 - 30$ at the right-hand side. By rows, the empirical distributions plotted correspond to the functional sample sizes $N = 50$ (first row), $N = 100$ (second row) and $N = 500$ (third row).

Regarding the empirical distribution of $\|f_{n,\hat{\theta}_N}(\cdot) - f_{n,\theta_0}(\cdot)\|_{L^1([-\pi,\pi])}$, plotted in Figures 12 and 13, under DPBS and IPBS of eigenvalues of the LRD operator, respectively, one can observe that IPBS of eigenvalues of the LRD operator slightly enlarges the supports of the empirical distributions with respect to DPBS of eigenvalues of the LRD operator. Also, more asymmetric patterns are observed, in some spherical scales, and, in some cases, closer to bimodality (see, e.g., right-hand side plot at the third row of Figure 13). Thus, under DPBS of eigenvalues of the LRD operator, more symmetry is observed in the empirical distribution patterns at most of the spherical scales, and the empirical distribution supports reduce faster, when the functional sample size increases. These differences are stronger at the highest resolution levels displayed (i.e., when parameter n increases).

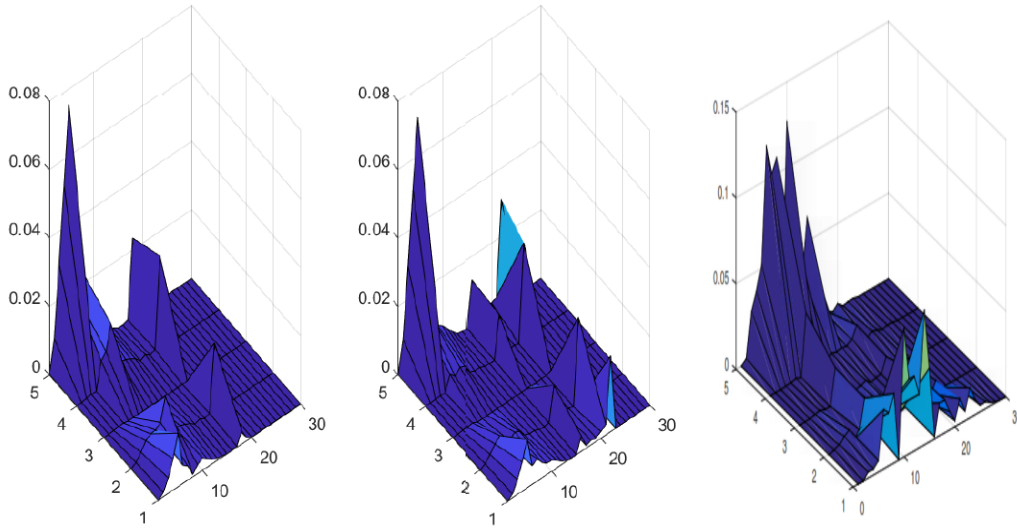


Figure 14: Under DPBS of eigenvalues of the LRD operator, the EMQE $\widehat{E} \left[(\widehat{\beta}_{n,j} - \beta_{n,j})^2 \right]$, $n = 1, 2, \dots, 30$, $j = 1, 2, \dots, 5$, based on $R = 100$ repetitions, are displayed for functional sample sizes $N = 50$ at the left hand-side, $N = 100$ at center, and $N = 500$ at the right hand-side.

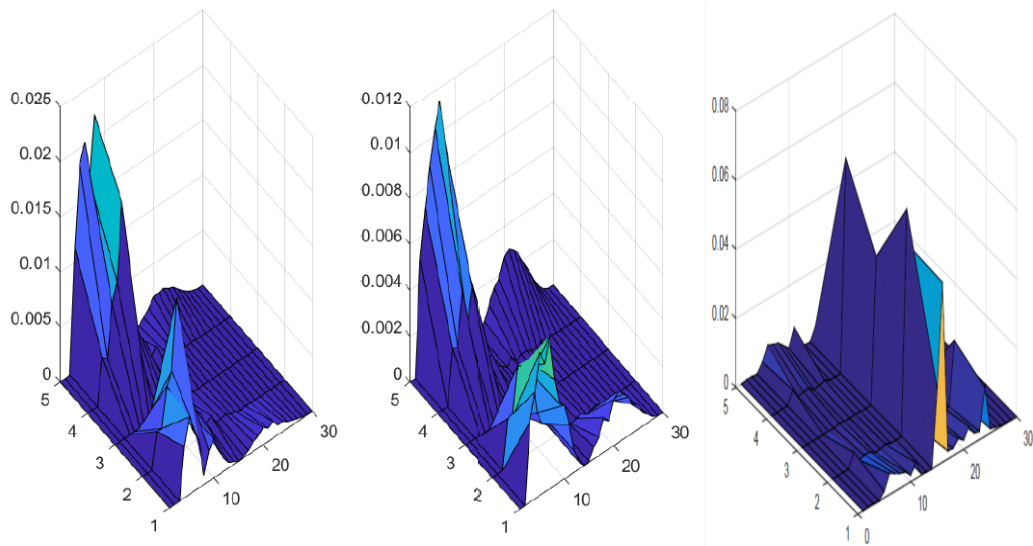


Figure 15: Under IPBS of eigenvalues of the LRD operator, the EMQE $\widehat{E} \left[(\widehat{\beta}_{n,j} - \beta_{n,j})^2 \right]$, $n = 1, 2, \dots, 30$, $j = 1, 2, \dots, 5$, based on $R = 100$ repetitions, are displayed for functional sample sizes $N = 50$ at the left hand-side, $N = 100$ at center, and $N = 500$ at the right hand-side.

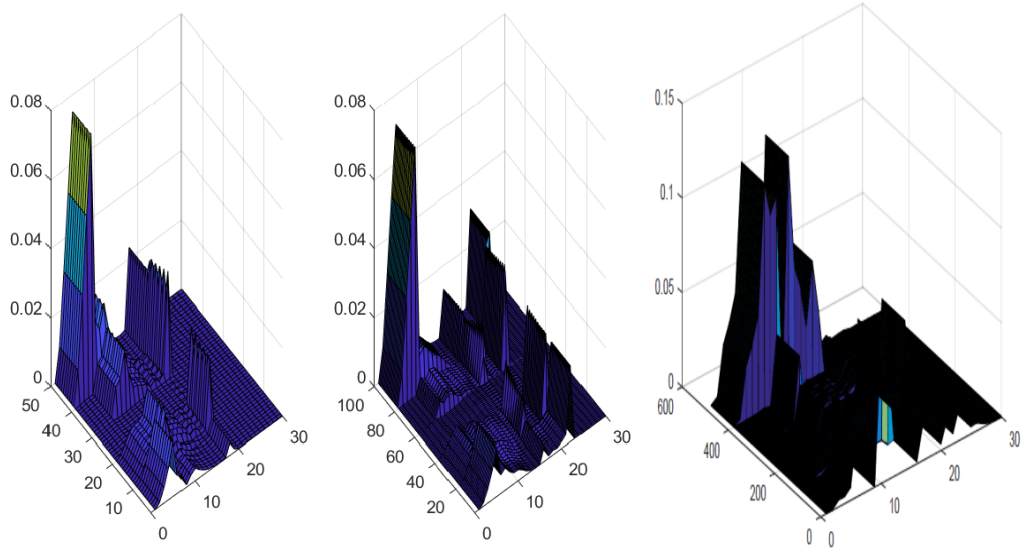


Figure 16: Under DPBS of eigenvalues of the LRD operator, the EMQE $\widehat{E} \left[(\widehat{Y}_n(t) - Y_n(t))^2 \right]$, $n = 1, 2, \dots, 30$, $t = 1, 2, \dots, N$, based on $R = 100$ repetitions, are displayed for functional sample sizes $N = 50$ at the left hand-side, $N = 100$ at center, and $N = 500$ at the right hand-side.

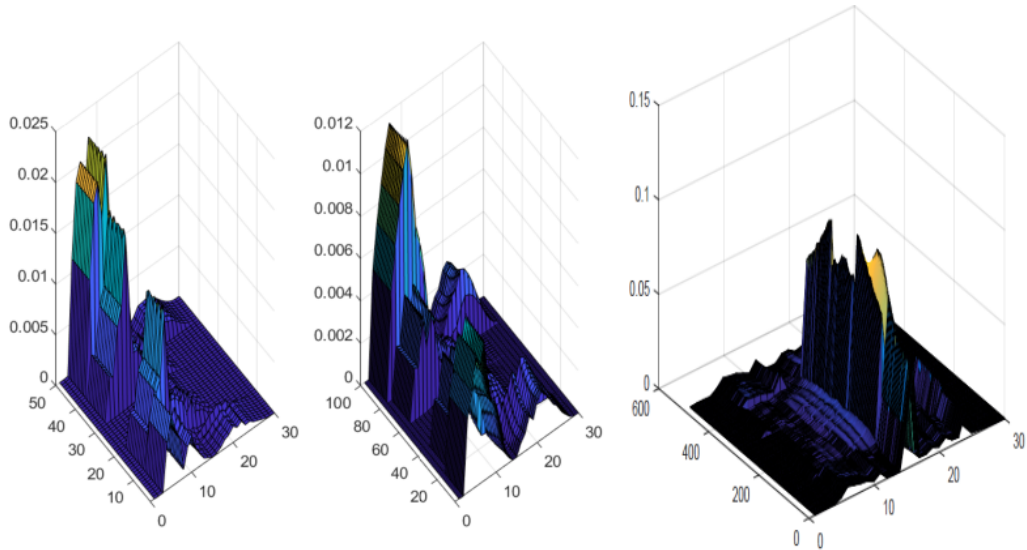


Figure 17: Under IPBS of eigenvalues of the LRD operator, the EMQE $\widehat{E} \left[(\widehat{Y}_n(t) - Y_n(t))^2 \right]$, $n = 1, 2, \dots, 30$, $t = 1, 2, \dots, N$, based on $R = 100$ repetitions, are displayed for functional sample sizes $N = 50$ at the left hand-side, $N = 100$ at center, and $N = 500$ at the right hand-side.

The plotted results in Figures 12 and 13 on the effect of parameters n (spherical scale), and N (functional sample size) on the empirical distribution of the statistics $\|f_{n,\hat{\theta}_N}(\cdot) - f_{n,\theta_0}(\cdot)\|_{L^1([- \pi, \pi])}$ lead to a stronger level of singularity in the estimated temporal functional spectrum under DPBS than under IPBS of eigenvalues of the LRD operator at coarser spherical scales (n small), due to a stronger smoothing effect of the latest (the IPBS of eigenvalues of the LRD operator scenario) at the zero frequency pole, for such coarser spherical scales. While at high resolution levels (n large), the opposite effect is observed regarding the stronger smoothing at high resolution levels of zero frequency pole under DPBS of eigenvalues of the LRD operator. These differences between both analyzed LRD operator eigenvalues scenarios are more pronounced when the functional sample size N increases, as it can be observed in Figures 14–17, regarding the highest EMQEs values displayed at coarser and high resolution levels in the sphere, associated with the plug-in estimation of β , and the corresponding prediction of the response \mathbf{Y} .

6 Conclusions and open research lines

This paper opens a new research line within the context of multiple functional regression analysis from strong-correlated in time functional data in a manifold \mathbb{M}_d . Particularly, the framework of connected and compact two-point homogeneous spaces is adopted. The formulated multiple functional regression model, with functional response, functional regression parameters and time-dependent scalar covariates, goes beyond the assumptions of weak-dependent, and the Euclidean setting usually adopted in the current literature in functional regression. The asymptotic properties of the GLS estimator of the \mathbb{M}_d -supported functional regression parameter vector β , when the second-order structure of the functional error term is known and unknown, are established. Indeed, these properties are obtained by applying the results derived in Ruiz-Medina, Miranda & Espejo [61]. In the GLS estimation of the \mathbb{M}_d -supported functional regression parameter vector β , the simulation study undertaken shows that, under totally specified model, i.e., when the second-order structure of the functional error term ε is known, the velocity decay and distribution of the singular values of the elements of the covariance operator family play a crucial role, in relation to the regularization effect induced by the slow decay in time of the covariance function. Note that this regularization effect also depends on the distribution of the eigenvalues of the LRD operator (in our analysis it depends on the DPBS and IPBS of eigenvalues of the LRD operator considered). The regularization effect acts on the inverse matrix sequence $\{\Lambda_n^{-1}, n \in \mathbb{N}_0\}$, involved in the linear filter defining the GLS parameter estimator. When the functional spectral-based plug-in estimation of

β is achieved under misspecified model, the increasing of the functional sample size leads to a more dense sampling at a neighborhood of the zero frequency pole, increasing the magnitude of the errors of the computed minimum contrast parameter estimator of the LRD operator. This effect is mitigated in part, in our study, by the stronger smoothing effect at spherical coarser scales under IPBS of eigenvalues of the LRD operator, while the opposite effect is observed under DPBS of eigenvalues of the LRD operator at such scales, with a stronger smoothing effect at high resolution levels in the sphere.

In a subsequent paper we address significance testing under this strong-dependence functional data scenario in the analyzed manifold multiple functional regression model (see, e.g., García-Portugués, González-Manteiga & Febrero-Bande [31], when i.i.d functional data are analyzed, and Ruiz-Medina [59] and Álvarez-Liévana & Ruiz-Medina [5] for weak-dependent functional data in the time series context).

Acknowledgements

This work has been supported in part by projects MCIN/ AEI/ PID2022-142900NB-I00, and CEX2020-001105-M MCIN/ AEI/10.13039/501100011033.

References

- [1] Acal, C. & Aguilera, A.M. (2023). Basis expansion approaches for functional analysis of variance with repeated measures. *Advances in Data Analysis and Classification*, **17**, 291–321. <https://doi.org/10.1007/s11634-022-00500-y>
- [2] Acal, C., Aguilera, A.M., Sarra, A., Evangelista, A., Battista, T.D. & Palermi, S. (2022). Functional ANOVA approaches for detecting changes in air pollution during the COVID-19 pandemic. *Stoch. Environ. Res. Risk Assess.*, **36**, 1083–1101. <https://doi.org/10.1007/s00477-021-02071-4>
- [3] Alegría, A., Bissiri, P.G., Cleanthous, G., Porcu, E., & White, P. (2021). Multivariate isotropic random fields on spheres: Nonparametric Bayesian modeling and L^p fast approximations. *Electronic Journal of Statistics*, **15**(1), 2360–2392. <https://doi.org/10.1214/21-EJS1842>
- [4] Álvarez-Liévana, J., López-Pérez, A., Febrero-Bande, M. & González-Manteiga, W. (2022). A goodness-of-fit test for functional time series with applications to Ornstein–Uhlenbeck processes. arXiv:2206.12821 (stat.ME).

- [5] Álvarez-Liébana, J. & Ruiz-Medina, M.D. (2017). The effect of the spatial domain in FANOVA models with ARH(1) error term. *Statistics and Its Interface*, **10**(4), 607–628. <https://dx.doi.org/10.4310/SII.2017.v10.n4.a7>
- [6] Álvarez-Liébana, J. & Ruiz-Medina MD. (2019). Prediction of air pollutants PM₁₀ by ARBX(1) processes. *Stochastic Environmental Research and Risk Assessment*, **33**, 1721–1736. <https://doi.org/10.1007/s00477-019-01712-z>
- [7] Andrews, G.E., Askey, R. & Roy, R. (1999). *Special Functions*, **71**. In *Encyclopedia of Mathematics and its Applications*. Cambridge University Press: Cambridge.
- [8] Aneiros-Pérez, G. & Vieu, P. (2006). Semi-functional partial linear regression. *Stat. Probab. Letters*, **76**(11), 1102–1110. <https://doi.org/10.1016/j.spl.2005.12.007>
- [9] Aneiros-Pérez, G. & Vieu, P. (2008). Nonparametric time series prediction: A semi-functional partial linear modeling. *J. Multivariate Anal.*, **99**(5), 834–857. <https://doi.org/10.1016/j.jmva.2007.04.010>
- [10] Aristizabal, J.P., Giraldo, R. & Mateu, J. (2019). Analysis of variance for spatially correlated functional data: Application to brain data. *Spatial Statistics*, **32**(100381). <https://doi.org/10.1016/j.spasta.2019.100381>
- [11] Benhenni, K., Hedli-Griche, S. & Rachdi M (2017) Regression models with correlated errors based on functional random design. *TEST*, **26**, 1–21. <https://doi.org/10.1007/s11749-016-0495-1>
- [12] Berkes, I., Horváth, L. & Rice, G. (2016). On the asymptotic normality of kernel estimators of the long run covariance of functional time series. *Journal of Multivariate Analysis*, **144**, 150–175. <https://doi.org/10.1016/j.jmva.2015.11.005>
- [13] Bosq, D. (2000). *Linear Processes in Function Spaces*. Springer: New York.
- [14] Caponera, A. (2021). SPHARMA approximations for stationary functional time series in the sphere. *Stat. Infer. Stoch. Proc.*, **24**, 609–634. <https://doi.org/10.1007/s11203-021-09244-6>
- [15] Caponera, A. & Marinucci, D. (2021). Asymptotics for spherical functional autoregressions. *Ann. Stat.*, **49**(1), 346–369. <https://doi.org/10.1214/20-AOS1959>

- [16] Cardot, H., Mas, A. & Sarda, P. (2007). CLT in functional linear regression models. *Probab. Theory Relat. Fields*, **138**, 325–361. <https://doi.org/10.1007/s00440-006-0025-2>
- [17] Cartan, E. (1927). Sur certaines formes Riemanniennes remarquables des géométries á groupe fondamental simple. *Ann Sci Éc Norm Supér*, **44**(3), 345–467. <https://doi.org/10.24033/asens.781>
- [18] Chiou, J.M. & Müller, H.G. (2007). Diagnostics for functional regression via residual processes. *Comput. Statist. Data. Anal.*, **51**(10), 4849–4863. <https://doi.org/10.1016/j.csda.2006.07.042>
- [19] Chiou, J.M., Müller, H.G. & Wang, J.L. (2004). Functional response models. *Statistica Sinica*, **14**(3), 659–677. <https://www.jstor.org/stable/24307411>
- [20] Crambes, C., Kneip, A. & Sarda, P. (2009). Smoothing splines estimators for functional linear regression. *Annals of Statistics*, **37**(1), 35–72. <https://doi.org/10.1214/07-AOS563>
- [21] Crambes, C. & Mas, A. (2013). Asymptotics of prediction in functional linear regression with functional outputs. *Bernoulli*, **19**(5B), 2627–2651. <https://doi.org/10.3150/12-BEJ469>
- [22] Cuevas, A. (2014). A partial overview of the theory of statistics with functional data. *Journal of Statistical Planning and Inference*, **147**, 1–23. <https://doi.org/10.1016/j.jspi.2013.04.002>
- [23] Cuevas, A., Febrero, M. & Fraiman, R. (2002). Linear functional regression: The case of a fixed design and functional response. *Canadian J. Statistics*, **30**(2), 285–300. <https://doi.org/10.2307/3315952>
- [24] Dette, H., Kokot, K. & Aue, A. (2020). Functional data analysis in the Banach space of continuous functions. *The Annals of Statistics*, **48**(2), 1168–1192. <https://doi.org/10.1214/19-AOS1842>
- [25] Dette, H. & Quanz, P. (2022). Detecting relevant changes in the spatiotemporal mean function. arXiv:2203.04716 (math.ST).
- [26] Febrero-Bande, M., Galeano, P. & González-Manteiga, W. (2017). Functional principal component regression and functional partial least-squares regression: an overview and a comparative study. *International Statistical Review*, **85**(1), 61-83. <https://www.jstor.org/stable/44840871>

- [27] Ferraty, F., Goia, A., Salinelli, E. & Vieu, P. (2013). Functional projection pursuit regression. *TEST*, **22**, 293–320. <https://doi.org/10.1007/s11749-012-0306-2>
- [28] Ferraty, F., Keilegom, I.V. & Vieu, P. (2012). Regression when both response and predictor are functions. *J. Multivariate Anal.*, **109**, 10–28. <https://doi.org/10.1016/j.jmva.2012.02.008>
- [29] Ferraty, F. & Vieu, P. (2006). *Nonparametric Functional Data Analysis: Theory and Practice*. Springer: New York.
- [30] Ferraty, F. & Vieu, P. (2018). Kernel regression estimation for functional data, 4. In *The Oxford Handbook of Functional Data Analysis*. Oxford University Press: Oxford, pp. 72–129. <https://doi.org/10.1093/oxfordhb/9780199568444.013.4>
- [31] García–Portugués, E., González–Manteiga, W. & Febrero–Bande, M. (2014). A goodness–of–fit test for the functional linear model with scalar response. *J. Comput. Graph. Statist.*, **23**(3), 761–778. <https://doi.org/10.1080/10618600.2013.812519>
- [32] Giné, E. (1975). The addition formula for the eigenfunctions of the Laplacian. *Advances in Mathematics*, **18**(1), 102–107. [https://doi.org/10.1016/0001-8708\(75\)90003-1](https://doi.org/10.1016/0001-8708(75)90003-1)
- [33] Goia, A. & Vieu, P. (2015). A partitioned single functional index model. *Computational Statistics*, **30**, 673–692. <https://doi.org/10.1007/s00180-014-0530-1>
- [34] Goia, A. & Vieu, P. (2016). An introduction to recent advances in high/infinite dimensional statistics. *Journal of Multivariate Analysis*, **146**, 1–6. <https://doi.org/10.1016/j.jmva.2015.12.001>
- [35] Guillas, S. (2002). Doubly stochastic Hilbertian processes. *J. Appl. Probab.*, **39**(3), 566–580. <https://www.jstor.org/stable/3216079>
- [36] Helwig, N.E., Shorter, K.A., Ma, P. & Hsiao–Wecksler, E.T. (2016). Smoothing spline analysis of variance models: A new tool for the analysis of cyclic biomechanical data. *Journal of Biomechanics*, **49**(14), 3216–3222. <https://doi.org/10.1016/j.jbiomech.2016.07.035>
- [37] Hörmann, S., Kidziński, Ł. & Hallin, M. (2015). Dynamic functional principal components. *J. R. Statist. Soc. B.*, **77**(Part 2), 319–348. <https://www.jstor.org/stable/24774739>

- [38] Hörmann, S. & Kokoszka, P. (2010). Weakly dependent functional data. *Ann Statist* **38**(3), 1845–1884. <https://doi.org/10.1214/09-AOS768>
- [39] Hörmann, S. & Kokoszka, P. (2013). Consistency of the mean and the principal components of spatially distributed functional data. *Bernoulli*, **19**(5A), 1535–1558. <https://www.jstor.org/stable/42919329>
- [40] Horváth, L. & Kokoszka, P. (2012). *Inference for Functional Data with Applications*. Springer: New York
- [41] Horváth, L., Rice, G. & Whipple, S. (2016). Adaptive bandwidth selection in the long run covariance estimator of functional time series. *Computational Statistics and Data Analysis*, **100**, 676–693. <https://doi.org/10.1016/j.csda.2014.06.008>
- [42] Hsing, T. & Eubank, R. (2015). *Theoretical Foundations of Functional Data Analysis, with an Introduction to Linear Operators*. In *Wiley Series in Probability and Statistics*. John Wiley & Sons: Chichester.
- [43] Kara–Terki, N. & Mourid, T. (2016). Local asymptotic normality of Hilbertian autoregressive processes. *Comptes Rendus Mathématique*, **354**(6), 634–638. <https://doi.org/10.1016/j.crma.2016.03.006>
- [44] Kokoszka, P., Reimherr, M. (2012). Determining the order of the functional autoregressive model. *J. Time Ser. Anal.*, **34**, 116–129. <https://doi.org/10.1111/j.1467-9892.2012.00816.x>
- [45] Leonenko, NN., Nanayakkara, R. & Olenko, A. (2021). Analysis of spherical monofractal and multifractal random fields. *Stoch. Environ. Res. Risk Assess.*, **35**, 681–701. <https://doi.org/10.1007/s00477-020-01911-z>
- [46] Li, D., Robinson, P.M. & Shang, H.L. (2019). Long–range dependent curve time series. *J. of the American Statistical Association*, **115**, 957–971. <https://doi.org/10.1080/01621459.2019.1604362>
- [47] Ma, C. & Malyarenko, A. (2020). Time varying isotropic vector random fields on compact two–point homogeneous spaces. *J. Theor. Probab.*, **33**, 319–339. <https://doi.org/10.1007/s10959-018-0872-7>
- [48] Marinucci, D. & Peccati, G. (2011). *Random fields on the Sphere. Representation, Limit Theorems and Cosmological Applications*. In *London Mathematical Society Lecture Note Series 389*. Cambridge University Press: Cambridge. <https://doi.org/10.1017/CBO9780511751677>

- [49] Marinucci, D., Rossi, M. & Vidotto, A. (2021). Non-universal fluctuations of the empirical measure for isotropic stationary fields on $\mathbb{S}^2 \times \mathbb{R}$. *Ann. Appl. Probab.*, **31**(5), 2311–2349. <https://doi.org/10.1214/20-AAP1648>
- [50] Mas, A. (1999). Normalité asymptotique de l'estimateur empirique de l'opérateur d'autocorrélation d'un processus ARH(I). *C. R. Acad. Sci. Paris*, **329**(10), 899–902. [https://doi.org/10.1016/S0764-4442\(00\)87496-0](https://doi.org/10.1016/S0764-4442(00)87496-0)
- [51] Morris, J.S. (2015). Functional regression. *Annual Review of Statistics and Its Application*, **2**, 321–359. <https://doi.org/10.1146/annurev-statistics-010814-020413>
- [52] Olaya-Ochoa, J., Ovalle-Muñoz, D.P. & Urbano-Leon, C.L. (2020). Functional analysis of variance of air pollution caused by fine particles. *Universitas Scientiarum*, **25**(1), 1–16. <https://doi.org/10.11144/Javeriana.SC25-1.faov>
- [53] Ovalle-Muñoz, D.P. & Ruiz-Medina, M.D. (2024). LRD spectral analysis of multifractional functional time series on manifolds. *TEST*, <https://doi.org/10.1007/s11749-023-00913-7>.
- [54] Panaretos, V.M. & Tavakoli, S. (2013a). Fourier analysis of stationary time series in function space. *Ann. Statist.*, **41**(2), 568–603. <https://doi.org/10.1214/13-AOS1086>
- [55] Ramsay, J.O. & Silverman, B.W. (2005). *Functional data analysis, 2nd edn. Springer Series in Statistics*. Springer: New York
- [56] Ruiz-Medina, M.D. (2011). Spatial autoregressive and moving average Hilbertian processes. *Journal of Multivariate Analysis*, **102**, 292–305. <https://doi.org/10.1016/j.jmva.2010.09.005>
- [57] Ruiz-Medina, M.D. (2012a). New challenges in spatial and spatiotemporal functional statistics for high-dimensional data. *Spatial Statistics*, **1**, 82–91. <https://doi.org/10.1016/j.spasta.2012.02.006>
- [58] Ruiz-Medina, M.D. (2012b). Spatial functional prediction from spatial autoregressive Hilbertian processes. *Environmetrics*, **23**(1), 119–128. <https://doi.org/10.1002/env.1143>
- [59] Ruiz-Medina, M.D. (2016). Functional analysis of variance for Hilbert-valued multivariate fixed effect models. *Statistics*, **50**, 689–715. <https://doi.org/10.1080/02331888.2015.1094069>

- [60] Ruiz–Medina MD (2022). Spectral analysis of long range dependence functional time series. *Fractional Calculus and Applied Analysis*, **25**, 1426–1458. <https://doi.org/10.1007/s13540-022-00053-z>
- [61] Ruiz–Medina, M.D., Miranda, D. & Espejo, R.M. (2019). Dynamical multiple regression in function spaces, under kernel regressors, with ARH(1) errors. *TEST*, **28**, 943–968. <https://doi.org/10.1007/s11749-018-0614-2>
- [62] Shen, Q. & Xu, H. (2007). Diagnostics for Linear Models with Functional Responses. *Technometrics*, **40**(1), 26–33. <https://www.jstor.org/stable/25471272>
- [63] Yao, F., Müller, H.G. & Wang, J.L. (2005). Functional linear regression analysis for longitudinal data. *Ann. Statist*, **33**(6), 2873–2903. <https://doi.org/10.1214/009053605000000660>
- [64] Zhang, X., Shao, X., Hayhoe, K. & Wuebbles, D. (2011). Testing the structural stability of temporally dependent functional observations and application to climate projections. *Electronic Journal of Statistics*, **5**, 1765–1796. <https://doi.org/10.1214/11-EJS655>.